UNIVERSIDADE D
COIMBRA

Saniat Jahan Sunny

TRIBOLOGICAL STUDIES OF CARBON-ALLOYED TRANSITION METAL DICHALCOGENIDE COATINGS SLIDING AGAINST ALUMINUM AT ELEVATED TEMPERATURES.

VOLUME 1

Dissertação no âmbito do Mestrado Conjunto Europeu em Tribologia de Superfícies e Interfaces orientada pelos Professor Albano Cavaleiro e apresentada ao Departamento de Engenharia Mecânica da Faculdade de Ciências e Tecnologia da Universidade de Coimbra.

Julho de 2022

1 2 9 0 FACULDADE DE CIÊNCIAS E TECNOLOGIA UNIVERSIDADE D COIMBRA

TRIBOLOGICAL STUDIES OF CARBON-ALLOYED TRANSITION METAL DICHALCOGENIDE COATINGS SLIDING AGAINST ALUMINUM AT ELEVATED TEMPERATURES.

Submitted in Partial Fulfilment of the Requirements for the Degree of Joint European Master in Tribology of Surfaces and Interfaces.

ESTUDOS TRIBOLÓGICOS DE REVESTIMENTOS DE DICALCOGENETOS METÁLICOS DE TRANSIÇÃO CARBONO-LIGADOS DESLIZANDO CONTRA O ALUMÍNIO A TEMPERATURAS ELEVADAS.

Author

Saniat Jahan Sunny

Advisor[s]

Prof. Albano Cavaleiro

Dr. Todor Vuchkov

Jury

President	**Professor Doutor Bruno Trindade**
	Professor at the Universidade de Coimbra
Vowel	**Doutor Manuel António Peralta Evaristo**
	Assistant Professor at Universidade de Coimbra
Advisor	**Professor Doutor Albano Cavaleiro**
	Professor at Universidade de Coimbra

1 2 9 0 UNIVERSIDADE D COIMBRA

tribos Joint European Master in Tribology of Surfaces and Interfaces Ljubljana • Leeds • Coimbra • Luleå

Coimbra, July 2022

ACKNOWLEDGEMENTS

Firstly, I would like to show my sincere gratitude to my supervisor, Prof. Albano Cavaleiro, and Dr Todor Vuchkov for guiding me and allowing me to be a part of the group. This would not have been possible without the continuous help of Dr Todor Vuchkov, at every step of the project. I am truly grateful to Dr Todor for teaching me a lot of new things and allowing me to work independently. Also, I would like to thank everyone at the Instituto Pedro Nunes for allowing me to work there.

I would like to thank the TRIBOS consortium and the European Commission for giving me this opportunity. I feel privileged to have received such a prestigious scholarship. This surely has been an amazing journey. I would like to thank Professor Mitjan Kalin, Professor Bruno Trindade, and Professor Ardian Morina for their help throughout the entire journey. I thank all the professors, lecturers, and colleagues from the University of Ljubljana, the University of Leeds, and the University of Coimbra.

I am grateful to everyone who has contributed to the completion of my thesis. This is a combined effort of all the amazing people I have come across who were generous enough to help. I would like to especially thank everyone from the Departamento de Engenharia Mecânica, the University of Coimbra, for their significant contribution to this thesis.

Finally, I would like to thank my mother and my family for their continuous support and motivation. Also, I thank all my friends who constantly supported me and encouraged me throughout the journey.

Abstract

The pursuit of lightweight design for automotive applications has lasted for many years and is still going strong. New and stricter emission standards, as well as the rising popularity of electric or hybrid vehicles—where the heavier weight of the batteries must be offset by lighter structures—are the key driving reasons. Maintaining or enhancing passenger safety while designing parts and structures with less weight is also crucial. The next generation of lightweight vehicle structures will be realized using materials with a high strength-to-weight ratio, such as high-strength aluminium alloys.

Potential methods to reduce wear and friction at the hot aluminium-tool steel interface include lubrication and surface engineering techniques. For the forming of aluminium, solid lubricants like hexagonal boron nitride (hBN) and graphite have been investigated. High-temperature applications are also increasingly being considered for polymer-based lubricants. The employment of protective coatings and the regulation of the tool surface topography are both surface engineering approaches. It has been discovered that surface roughness is a key factor at the beginning of aluminium transfer to the counter-surface. Thin PVD and CVD coatings are being researched increasingly as a potential galling remedy. CrN and DLC coatings, among others, are known to lessen adhesion when sliding on aluminium.

The purpose of this study is to better understand how aluminium behaves tribologically when it slides against tool steel at elevated temperatures. This current study aims to develop three different coatings of W-S-C varying the carbon content and understanding its influence of it on morphology, structure, and mechanical properties. Deposition of the coatings was done by magnetron sputtering. The carbon percentage of the coatings varied from around 6% to 35%. To understand the tribological characteristics of the coating reciprocating ball-on disk experiments were carried out. Experiments were conducted at RT, 200°C, and 400°C.

It was found that coating on the tool surface can significantly reduce the galling of aluminium and the wear on the tool surface. However, increasing the percentage of carbon also has an adverse effect. It was found that carbon % of around thirty serves the purpose best. Coatings with carbon of around 30% showed excellent galling resistance at elevated temperatures.

Keywords: TMD, W-S-C, Aluminium galling, magnetron sputtering,

Resumo

A procura de design leve para aplicações automotivas tem vindo a aumentar há muitos anos e continua a ser forte. Novas e mais rigorosas normas de emissões, bem como a crescente popularidade dos veículos eléctricos ou híbridos - onde o peso mais pesado das baterias deve ser compensado por estruturas mais leves - são as principais razões de condução. Manter ou melhorar a segurança dos passageiros ao mesmo tempo que se concebem peças e estruturas com menos peso é também crucial. A próxima geração de estruturas de veículos ligeiros será realizada utilizando materiais com uma elevada relação força/peso, tais como ligas de alumínio de alta resistência.

Os métodos potenciais para reduzir o desgaste e o atrito na interface alumínio-aço quente das ferramentas incluem técnicas de lubrificação e engenharia de superfícies. Para a formação de alumínio, foram investigados lubrificantes sólidos, tais como nitreto de boro hexagonal (hBN) e grafite. As aplicações a altas temperaturas estão também a ser cada vez mais consideradas para lubrificantes à base de polímeros. A utilização de revestimentos protectores e a regulação da topografia de superfície de ferramentas são ambas abordagens de engenharia de superfícies. A rugosidade da superfície foi considerada como um factor chave para iniciar a transferência do alumínio para a superfície do contador. Os revestimentos finos de PVD e CVD estão cada vez mais a ser investigados como um remédio potencial para a abrasão. Os revestimentos CrN e DLC, entre outros, são conhecidos por diminuírem a aderência quando deslizam sobre o alumínio.

O objectivo deste estudo é compreender melhor como o alumínio se comporta tribologicamente quando desliza contra o aço-ferramenta a temperaturas elevadas. Este estudo visa desenvolver três revestimentos W-S-C diferentes, variando o conteúdo de carbono e compreendendo a sua influência na morfologia, estrutura, e propriedades mecânicas. Os revestimentos foram depositados por pulverização catódica. A percentagem de carbono dos revestimentos variou de cerca de 6% a 35%. Para compreender as características tribológicas do revestimento, foram realizadas experiências com discos de esferas de reciprocidade. Foram realizadas experiências a RT, 200°C, e 400°C.

Verificou-se que o revestimento na superfície da ferramenta pode reduzir significativamente a gripagem do alumínio e o desgaste na superfície da ferramenta. No entanto, o aumento da percentagem de carbono tem também um efeito adverso. Verificou-se que a percentagem de carbono de cerca de trinta foi a que melhor serve o propósito. Revestimentos com carbono de cerca de 30% mostraram uma excelente resistência do feltro a temperaturas elevadas.

Keywords: TMD, W-S-C, galling de alumínio, pulverização de magnetrões

[LIST OF FIGURES]

[LIST OF TABLES]

[ACRONYMS/ABBREVIATIONS]

AFM	Atomic force microscopy
AISI	American Iron and Steel Institute
CFUBMS	Closed-field unbalanced magnetron sputtering
COF	Coefficient of friction
CO_2	Carbon dioxide
CrN	Chromium nitride
CVD	Chemical vapor deposition
DC	Direct current
DCMS	Direct current magnetron sputtering
DEM	Departamento de Engenharia Mecânica
DLC	Diamond-like carbon
EDS	Energy dispersive spectroscopy
FESEM	Field emission scanning electron microscope
GIXRD	Grazing incidence X-ray diffraction
IPN	Instituto Pedro Nunes
ISO	International Organization for Standardization
MoS_2	Molybdenum disulphide
NA	Numerical aperture
p-DC	Pulsed direct current
PTFE	Polytetrafluoroethylene
PVD	Physical vapor deposition
RF	Radiofrequency
RH	Relative humidity
RT	Room temperature
SAE	Society of Automotive Engineering
SEM	Scanning Electron Microscopy
TEM	Transmission electron microscopy

TiC	Titanium carbide
TMDs	Transition Metal Dichalcogenides
TMD-C	Carbon doped transition metal dichalcogenide
WC	Tungsten carbide
WDS	Wavelength dispersive spectroscopy
WS_2	Tungsten disulphide
W-S-C	Tungsten-Sulfur-Carbon
XPS	X-ray photoelectron spectroscopy
3D	Three-dimensional

[SYMBOLS]

C° – Degrees Celsius

d - Scar diameter

k – Specific wear rate

E – Modulus of Elasticity

F_n -Normal force

H – Hydrogen

H - Hardness

C – Carbon

N – Nitrogen

Ar – Argon

V_w -Wear volume

W_r - Specific wear rate

Table of Contents

CHAPTER 1

1. INTRODUCTION

Tribology is the discipline of studying interacting surfaces in relative motion, making friction and wear one of the most pressing technological concerns today, especially given the wide range of conceivable working settings [1]–[3]. Many industrial applications operate in harsh environments, causing components to break prematurely, especially at elevated temperatures. Solid lubricants are one of the most promising methods for reducing friction in high-temperature environments and improving the manufacturing process of automotive alloys, as liquid lubricants degrade rapidly under such conditions[4].

Friction is an unavoidable part of the motion, and it cannot be diminished from the system but only be reduced. Any relative motion between two surfaces will encounter friction. However, a considerable amount of resources as well as the lifetime of equipment can be increased by the careful selection of a correct lubricant. A lubricant's job is to keep opposing surfaces from coming into close contact with one another, preventing mutual damage. Liquid lubricants have been used to minimize friction, suppress, or limit contact pressure, and facilitate sliding between solids. They also allow for a reduction in the amount of heat created by friction. In many circumstances, the presence of liquid is neither practical nor desirable, and it may even be restricted in order to avoid contamination of the product in question. This is especially true in vacuum conditions, systems requiring extremely tight tolerances, and applications involving materials with incompatibility issues. Thus, establishing functional surfaces by the application of coatings capable of providing self-lubricating qualities and acceptable contact angles in relation to lubricants is a potential option for abolishing or at least lowering the need for liquid lubricants.

Liquid lubricant deterrence is a significant difficulty in the industrial business whenever two solids move against each other. Consider the variety of engine components, as well as the broad range of materials processing procedures such as stamping and cutting. As a result, designing and developing self-lubricating coatings has become a popular topic of applied study. Sputter-deposited hard and wear-resistant coatings have been produced over several decades and applied to the surface of components to increase their surface tribological qualities. To protect the surface of items, various coatings such as nitrides, carbides, oxides, and borides are now commercially available [5]. To increase the performance and lifetime of various tribological components, solid lubricant coatings such as diamond-like carbon (DLCs), transition metal dichalcogenides (TMD), and WC have been introduced. Due to their limited oxidation resistance, they degrade in humid environments and/or oxidized quickly at elevated temperatures.

In today's world, high-performance materials are frequently needed to perform under extreme conditions, resulting in significant tribological difficulties. Due to the commercialization of a large number of diverse mechanical components, the automobile sector is acknowledged to have a noteworthy influence on the global economy. Many mechanical devices require prior lubrication before being assembled. Tools should have a mix of low friction and specific wettability features for an efficient and long-lasting lubricant application. One such material is Aluminium and its alloys. However, a particular problem arises when aluminium and its alloys are subjected to sliding or any form of motion. The galling of aluminium is a severe type of adhesive wear that is further accelerated by the influence of high temperature (350-450°C) seems to be a major topic of concern.

W-S-C coatings that are self-lubricating are ideal for use on mechanical components that are subjected to dry sliding under a variety of working conditions. In many cases it is found Carbon alloyed transition metal dichalcogenide coatings could be one such approach to reduce the friction significantly. In this thesis carbon alloyed WS_2 coatings performance along with tribological properties will be put under test. These coatings already have a reputation of working seamlessly with an upper-temperature range of 400°C-450°C. Tungsten disulfide (WS_2) is a transition metal dichalcogenide (TMD) compound with a highly anisotropic crystal structure that is frequently employed as a solid lubricant.

Hence, the goal of this thesis is to investigate the high-temperature performance of TMD-C coatings sliding against a specified aluminum alloy at temperatures as high as 450°C.

Framework

This project is being conducted on behalf of the University of Coimbra in partnership with the Instituto Pedro Nunes (IPN, LED & MAT), Coimbra. The project's objectives and goals are extremely relevant to the industry and have been developed accordingly.

The title of the project is "Tribological studies of carbon-alloyed transition metal dichalcogenide coatings sliding against aluminum at elevated temperatures" is performed as a master thesis for the fulfillment of the requirement of Joint European Master's Degree in Tribology of Surfaces and Interfaces. The opening portion of this work describes the nature and outline of the challenges encountered in the industry, as well as the type of work conducted in this project to address them. The following section includes a detailed description of current knowledge and advances in the field, which includes not only the physical definition of the problem but also existing applications, established paths, and gaps in understanding of the phenomenon, as well as the study's established objectives, final findings, and all established protocols, methods, and selected materials.

Thesis Organization

There are six chapters in this draft of the thesis. The purpose of this study, which is outlined in Chapter 1, is to highlight the need for novel lubricating techniques and give an overview of TMDs. In Chapter 2, the function of solid lubricants, the usage of coating to protect surfaces and achieve desirable qualities, and a brief description of the structure and doping of TMDs are all presented succinctly. Also includes a description of W-S-C coatings' current state of development. The concept of aluminium galling and the elements affecting it are also introduced in Chapter 2. The equipment and settings utilized to conduct the experimental work are briefly described in Chapter 3. Additionally covers the method used to conduct experiments. The findings and analysis of all the tests conducted are presented in Chapter 4. Chapter 5 contains the conclusion remarks of the thesis. Chapter 6 presents the scope of any future improvement that can be done.

CHAPTER 2

2. STATE OF THE ART

The extraordinary lubricating and tribological properties of self-lubricating coatings such as TMDs are an interesting topic of research. Over the past decades, numerous works have been conducted to enhance the understanding of this particular coating. In this section of the report, the present understandings of solid lubricants, self-lubricating coatings, TMD etc. are discussed extensively. Although more study has been done on molybdenum disulfide (MoS_2), the attention is now turning to tungsten disulfide (WS_2) because of its greater oxidation resistance and thermal stability even at elevated temperature[6].

2.1 Coatings

Many factors are considered while designing mechanical components, many of which include mechanical bulk qualities and how to minimize fatigue, fracture, or yielding. Unfortunately, materials that are suited in these respects are not always useful in terms of tribology. Modifying the surface, such that the materials in the bulk and on the surface are optimal for their respective roles, is a frequent approach to this problem. Applying a coating on the surface is one technique to change it.

Even if the coating is just a few micrometers thick (i.e., a fraction of the diameter of a human hair), it can substantially alter the surface's characteristics. The major focus of this research is on low-friction coatings with adequate wear resistance. Coating and (thin) film are interchangeable synonyms, although in this article, coating is used to prevent confusion with tribofilms.

It's also feasible to tell the difference between the coating's bulk and surface qualities with a closer look. By reducing the area of contact sites and the depth of asperities, a firm surface can reduce friction. However, in order to reduce friction, the interface's shear strength should be low, which is common for soft materials. A possible approach is a hard surface with strong load-bearing capability and a very thin covering of a soft, easily sheared substance. A tribofilm, which may be as thin as nm and still provide low friction, can be used as the low-friction material. For example, lubricating graphite is created as a tribofilm on top of a hard and wear-resistant coating in carbon-based coatings. This study applies a similar idea to the fabrication of WS_2 tribofilms.

As previously stated, the local condition in a tribological interaction is frequently intense, and the likelihood of material changes is significant. Triboactive coatings are those that

spontaneously create and sustain tribofilms with desirable qualities. This means that they alter and generate advantageous tribofilms as a result of chemical interactions, material transfer, or structural rearrangements and that they do so preferably throughout the component's lifespan to keep the tribofilm intact. In the current study, this method was employed to create low-friction WS_2 tribofilms in a tribological contact by creating nanocomposite or amorphous coatings.

2.2 Transition metal dichalcogenides (TMD)

Transition metal dichalcogenides are a type of material made up of atoms of transition metals (such as Mo and W), and atoms of dichalcogenide (such as S, Se, and Te). Due to their exceptional performance as solid lubricants in dry air or vacuum, the tribological properties of transition metal dichalcogenides (TMD), such as molybdenum and tungsten disulfides and di selenides, have been investigated for decades.

2.2.1 Structure and Properties of TMD

The general formula for transition metal dichalcogenides (TMDs) is MX_2 (M = W, Mo; X = S, Se). The hexagonal crystal structure's high anisotropy, which combines strong intra-planar interactions between chalcogenide and metal atoms with weak bonding between neighbouring metal chalcogenide layers, is thought to be responsible for its self-lubricant properties. As a result, the inter-lamellar bindings may be readily broken, allowing for easier sliding, while the intra-planar bonds assist prevent asperity penetration [7]. TMDs have a similar lamellar structure to graphite, but their tribological characteristics differ owing to various reactivity with the environment. Low graphite friction is caused by hydrogen saturation of dangling bonds; as a result, graphite has low friction in humid air and high friction in vacuum [8].

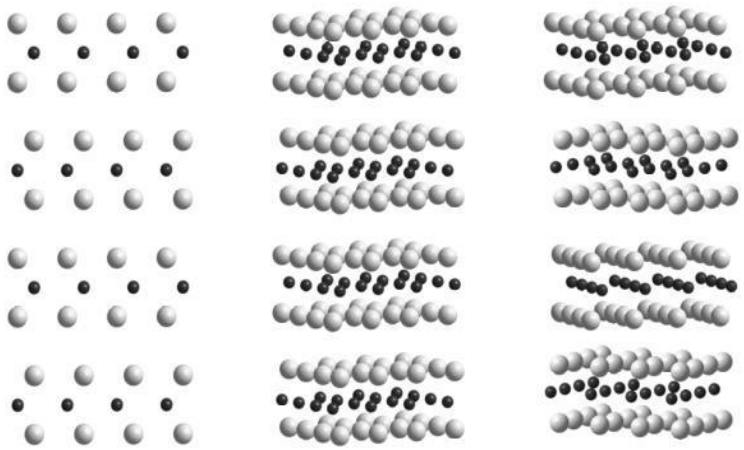

Figure 2.1: Structure of WS_2 in 2D and 3D (left and middle), as well as turbostratically layered WS_2 in 3D. (right). W atoms are dark grey, S atoms are light grey, and the c axis is the paper's vertical line[63].

The presence of oxygen or air humidity, on the other hand, is deleterious, causing high friction and wear rates [9]. As a result, sputtered TMD films' columnar architecture and porous structure severely limit their potential to operate as a self-lubricant coating in humid air[10], [11].TMDs in their most common form have a hexagonal symmetry due to the stacking sequence of two sandwich layers, which is designated as 2H-MeX_2. When three sandwich layers are stacked in a row, the lesser-known rhombohedral shape 3R-MeX_2 emerges [12]. When the sandwich layers are parallel but rotated more or less arbitrarily along the c axis, this is known as turbostratic stacking as shown in Figure 2.1.

Because TMD coatings may create a tribolayer on contact, it is generally established that they give minimal friction [13], [14]. The tribolayer is made up of pure crystalline TMD with a plane parallel to the sliding surface (002). This positioning is good for reducing friction and oxidation. The creation of this low friction tribolayer often signals the conclusion of the system's running-in period, following which the coefficient of friction achieves a stable state. However, with carbon alloyed TMD coatings, tribolayer production on contact is not always assured or enough, extending the system's run-in duration. Because the coating may not have enough TMD material to sustain the creation of the tribolayer as the carbon concentration increases, this is the case. As a result, when integrating carbon into a TMD coating, the chemical composition must be balanced in order to improve the friction-reducing capabilities without sacrificing mechanical qualities. For tribological applications, the hexagonal crystal structure, 2H, is very significant. This crystal structure maintains sixfold symmetry, which means that when rotated by one-sixth turn, the crystal appears the same. Each metal atom in hexagonal TMD has six equidistant dichalcogenide atoms around it, and each dichalcogenide atom has three equidistant metal atoms surrounding it. A laminar structure may also be seen in the hexagonal crystal structure. The hexagonal crystal structure's properties contribute to its lubricious nature. Other crystal forms can also be employed for friction-reducing purposes, even though the hexagonal TMD is the most effective for tribological applications.

Hardness and adhesion are the two most essential fundamental qualities for tribological coatings since they are directly connected to the coating's predicted durability. Hardness has a direct relationship to the coating's lifetime since it reduces wear damage. The hardness of pure TMD materials ranges from 0.3 to 2 GPa, while the actual value depends on a number of parameters including the deposition process used, morphology, and stoichiometry (X/M ratio) [13]. Nonetheless, this value is inadequate for tribological applications. Diamond-like-carbon, another common material for low-friction coatings, with a hardness of up to 70 GPa [15]. TMD alloyed with stronger materials like titanium, on the other hand, has shown to increase hardness by an order of magnitude.

The coating's and substrate's adhesion must be strong enough to prevent the coating from slipping away during sliding contact. TMD has a poor adherence to the most popular tribological substrates, such as steel [16]. By placing an interlayer between the TMD coating and the substrate, the adhesion between them may be improved. The interlayers of titanium and chromium have been employed with varying degrees of effectiveness.

2.2.2 Doping of TMD Films

Pure TMD coatings have been co-deposited with materials known to have greater mechanical qualities in order to increase their mechanical properties. Metals, on the other hand, not only have poor friction qualities, but they are also susceptible to oxidation. Adding a non-metallic element, such as carbon (C) or nitrogen (N), seems to be a realistic and promising option, and these elements have been co-deposited with TMDs. These elements' proclivity to create oxides isn't a problem because their oxides are gaseous and flee contact without harming the TMD coating [17]. When TMD coatings are alloyed with non-metallic elements, there is always the chance that the doping elements will react with transition metals or dichalcogenides, resulting in a larger non-TMD content in the coating. In the late 1990s, many scientific groups began investigating a novel coating idea based on the alloying of transition metal dichalcogenides (TMDs) with carbon [18]. Initially, they hoped to combine TMDs' superior frictional performance in a vacuum and dry air with the tribological features of diamond-like carbon (DLC) coatings [18]. Along with the aforementioned modifications, it was also predicted that the coating's compactness in relation to TMDs would improve, as well as the mechanical characteristics, notably the hardness.

There have been studies on the impact of chemical composition on the tribological performance of carbon alloyed TMD coatings in recent years. The most ideal composition for W-S-C coating, according to Polcar and Cavaleiro's investigations in the 2000s, was 50 at. % Carbon and 27 at. % Sulfur, with a S/W ratio of roughly 1.2 and 1.3 [19], [20]. Recent research suggests, however, that coatings with a reduced carbon concentration may have beneficial features as well. Furthermore, these latest investigations demonstrate that a higher S/W ratio is preferable to the low S/W ratios seen in Polcar and Cavaleiro's research.

Vuchkov et al. evaluated the tribological performance of W-S-C coatings at 50 at. % Carbon with S/W ratios ranging from 1.2 to 1.69 in research published in 2020 [21]. The study found that two coatings with equal sulfur content (27 and 28 at. %) but differing S/W ratios, one at 1.56 and the other at 1.4, performed differently. During the tribotest, the coating with a S/W ratio of 1.4 was completely worn down, but the coatings with higher S/W ratios attained a steady-state COF of 0.1 – 0.15. The coating with the greatest S/W ratio outperformed the others in the testing, requiring the least run-in time before reaching a steady-state COF of 0.12 – 0.15.

Raman examination of the best-performing coating's wear scars revealed strong peaks that belonged to crystalline WS_2. The coatings with low S/W ratios also failed to create a tribolayer, adding to their failures throughout the test, according to the author. The S/W ratio, together with the sulfur concentration, plays a critical role in the production of lubricous tribolayers in W-S-C coatings, according to this research.

The findings of Vuchkov's study are similar to those of Cao et al., who published a study in 2019. High S/W and sulfur concentrations are also desired in the quest of increased performance for W-S-C coatings, according to Cao's research. Cao's study found that the highest performing W-S-C coatings had a high sulfur content of 50 at. % and a 1.6 S/W ratio [22], similar to Vuchkov's findings. In Cao's investigation, Raman examination of the wear track of the best performing coating revealed strong WS_2 peaks, suggesting the formation of an abundant tribolayer on the surface. The best W-S-C coating in this investigation had just 20 at. % Carbon, indicating that low-carbon coatings can still perform well in tribological applications. Another research published in 2020 by Yaqub et al. supports this conclusion. The performance of Mo-Se-C coatings with Carbon content of less than 30 at. % was studied in Yaqub's work. The decreased Carbon concentration contributed to the ease of tribolayer production, shortening the coating's running-in duration, according to the findings [25]. The importance of composition in the performance of Carbon alloyed TMD coatings has been demonstrated in previous research. In general, a high X/M ratio is preferred since it correlates with greater TMD crystallinity [21]. Furthermore, a greater TMD content (achieved by lowering the carbon concentration) is advantageous since it stimulates the creation of tribolayer, minimizing the system's running-in period. It should be remembered, however, that a lower carbon percentage also means a lower hardness of the coating.

2.2.3 TMD and Tribology

TMD has been studied extensively for its potential in tribological applications for decades. TMD materials have the potential to function as lubricant additives. Though conventional additive chemicals such as zinc dialkyldithophosphate (ZDDP) perform well as lubricant additives, TMD materials have an inherent advantage as a lubricant additive. TMD materials have better chemical stability and lower toxicity, making them a better alternative with regard to the environmental impact. MoS_2 and WS_2 have been singled out for their effectiveness as lubricant additives[22]. In reality, molybdenum dithiocarbamate (MoDTC), a well-known traditional lubricant addition, operates by utilizing the benefits of a TMD. The in-situ creation of MoS_2 layers is the key mechanism of MoDTC for friction reduction. This demonstrates that TMD materials can increase lubricant performance by reducing friction.

TMD materials employed as surface coatings are classified as solid lubricants. A grasp of the mechanism of metallic friction should be created first in order to better comprehend how solid lubrication achieves friction reduction. Though friction is commonly thought of as a surface phenomenon, the frictional force and type of sliding between metals are intricately connected to the metals' bulk qualities, such as hardness and melting points. The frictional force between contacting metals is primarily caused by (1) shearing of metallic connections caused by contacting bodies adhesion and welding, and (2) dragging and ploughing of the softer metal's surface imperfections [23]. Solid lubricants lower friction by reducing the area over which metallic connections form and break, as well as the strength of adhesion at these junctions [23]. To isolate the metal surface below, an efficient solid lubricant should have an easily shearing layer (such as TMD materials) on top of a load-supporting layer with high hardness.

TMD nanocomposites appear to be the next step in the development of TMD as a tribological covering. This is due to the limited load-bearing capability of pure TMD materials, which makes them susceptible to wear degradation. Aside from mechanical features, pure TMD material's sensitivity to oxidation may limit their performance in tribological applications. TMD thin films have been found to oxidize in the air [22]. Because the edges of dichalcogenide atoms (such as sulfides and selenides) can react with nearby molecules to produce oxides [24], this is the case. In the TMD system, surface oxides have been shown to enhance friction [25]. With all of the inherent disadvantages of pure TMD materials, reinforcing TMD with other materials is required to fully exploit their tribological potential.

2.2.4 Tribofilm formation

To achieve the desired level of extremely low friction in case of dry contacts, it is crucial for the formation of tribofilm. These newly formed tribofilm are extremely soft and have exceptionally low shear strength, this is the key mechanism for low friction. When load is applied to the basal plane, they align themselves in the direction applied load to form a tribofilm. As deposited coatings have been found to have planes oriented in undesirable direction. When load is applied, the newly generated tribofilm causes the (002) shearing plane to shift along the sliding direction. While running in period, some of tribofilm may dispense along with impurities from the contact proving beneficial for the system. In the beginning the coefficient of friction and wear is high as asperities are being deformed but once a uniform tribofilm is formed the system becomes independent of the need of repeated lubrication as in fluid-based systems[26]. The opposing repulsion between TMD layers is primarily responsible for the coating's wear and shearing. The coating from below later evolves to refill the TMD tribofilm by reorientations under sliding contact, following some initial wear. The transfer of coating to the counter body and reorientation affects the friction coefficient. However, real-world conditions are not ideal,

and the atmosphere's influence on humidity reduces the low friction and wear characteristics of TMDs. In any case, running-in time is the amount of time needed for tribofilm formation. These factors include the coating's composition, stoichiometry, hardness, roughness, and operating conditions such sliding speed, number of laps, moisture content, load, and temperature. When the tribofilm has developed, the configuration acts as a fluid system. The planes along which simple shearing is occurring cannot be distinguished at this time. Shearing over the low shear strength basal planes causes the sliding to occur only inside the tribofilm. As a result of these tribofilm forms, TMDs seem to be a better alternative to liquid lubricants because they can aid with problems like cold start and fluid volatility[27].

2.2.5 Limitations of TMD films

TMD films, on the other hand, have flaws that must be addressed in order to fully realize their potential. It is impossible to employ pure TMD films produced by conventional magnetron sputtering under room settings because magnetron sputtering invariably results in a chaotic structure. Low-friction conspicuous orientation, (0002), can only be accomplished for a very thin layer with a thickness of a few tens of nanometers [7]. When TMD films slide in the air, they are known to create metal oxides and are very vulnerable to environmental threats. The presence of WO_3-X and MO_3-X oxides causes an increase in friction [28]–[30]. The Van der Waals force in basal plane (0002) is more resistant to environmental damage than the reactive plane (112) [31]. TMDs with basal planes parallel to the surface are therefore resistant to oxidation[32]. TMD films, due to their columnar shape, are very porous, allowing oxygen, water, and other reactive species to easily infiltrate the film [32]. Storing TMD films in an open environment is also known to have negative impacts on their tribological characteristics. When compared to rival low-friction coatings like diamond-like carbon (DLC), TMD films have low hardness, ranging from 0.3 to 2 GPa depending on stoichiometry, shape, and deposition circumstances [32]. TMD films do not stick well to steel substrates, but a thin metallic interlayer, such as Ti or Cr, improves adhesion between the film and the substrate [33]. Diselenides have been demonstrated to be more resistant to water and oxygen assaults in studies. TMD films are removed from surfaces when exposed to high contact pressures, a characteristic related to the films' limited load-bearing capability, which is a direct outcome of their morphology and low adhesion [33]. Material transfer to the counter-body might be another disadvantage in many applications.

Reduced water in residual chamber atmosphere to reduce oxygen content in the film [34], variation of deposition temperature[35] or gas pressure, and other approaches that have slightly improved TMD tribological behavior are among the various countermeasures applied to remedy the aforementioned limitations. The primary difficulties, however, have persisted, and pure sputtered TMD films are now only used in vacuum [36].

2.3 Magnetron Sputtering

Sputtering is the process of atoms ejecting from a substance after being bombarded by energetic particles. This procedure allows for the deposition of coatings if these particles are allowed to condense on a substrate. In the presence of ions from a sputtering gas, a source material, or a target, releases atoms. In a vacuum chamber, the liberated atoms are subsequently placed on a substrate. To allow the sputtered atoms to reach the substrate surface, a vacuum chamber is employed. The most common sputtering gas is argon (Ar). The discharge causes the formation of an Ar+ ion plasma, which is maintained by the ionization of Ar atoms. The employment of a magnetic field near the target to boost plasma density is known as magnetron sputtering. As a result, an eroded zone forms on the target, and the target's atoms are ejected from an erosion zone also termed racetrack due to its appearance.

The magnetron sputtering system produces high purity film at a high deposition rate when compared to DC and RF diode sputtering systems. This is due to the fact that magnetron sputtering is a low-pressure method, with interior chamber pressures as low as 10.3 mbar (compared to 10.2 mbar of DC diode sputtering). Magnetic fields are used on the cathode in magnetron sputtering devices. Secondary electrons emitted during sputtering will be entrapped by the ensuing magnetic field. The secondary electrons will gyrate around the magnetic field, increasing the chances of colliding with the neutral argon gas. As a result, a higher likelihood of ionization of the argon gas is attained, resulting in a denser plasma. A faster deposition rate is predicted with higher-density plasma.

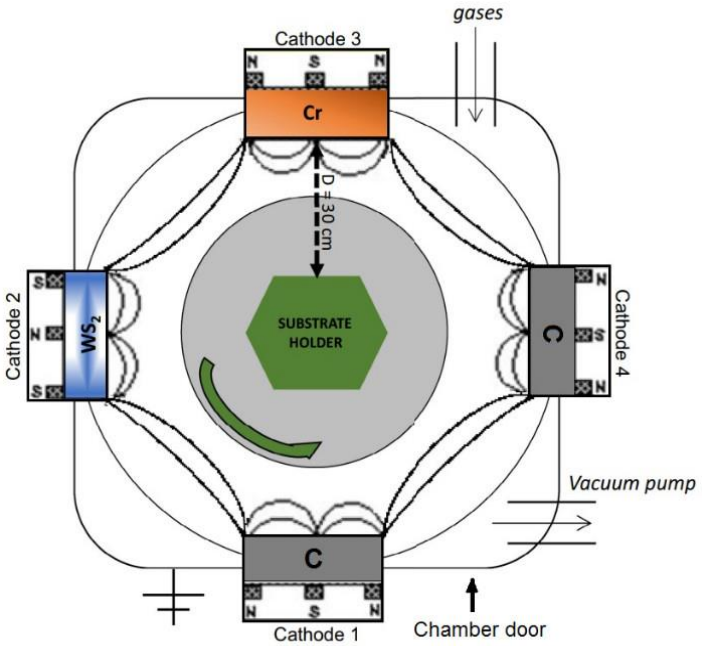

Figure 2.2: Schematic representation of the deposition unit with arrangements of the target[70].

The different process parameters influence the behavior of atoms as they travel from the target to the substrate's surface. Because this varies depending on the atom, the composition of a multi-element coating is entirely reliant on the method. In the case of a complex target, the composition of the deposited coating often differs from that of the target. During gas phase transport, the size and mass of sputtered atoms impact their behavior in collision with other atoms and their chance of reaching the substrate. However, the sputtered species are usually neutral atoms but can be ions as well. Because the sticking coefficient varies per element, not all sputtered atoms that reach the substrate surface are actually deposited.

Balanced/conventional magnetron sputtering, and unbalanced magnetron sputtering are the two forms of magnetron sputtering. One pole of the magnet is placed at the target material's central axis, while the other pole is placed on the edges in a balanced magnetron sputtering system. All magnetic field lines between the central and edge poles are closed in this design. In an unbalanced magnetron sputtering system, on the other hand, the strengthening or weakening of one of the poles directs certain magnetic field lines toward the substrate [37], Figure 2.2 shows a typical unbalanced magnetron sputtering unit with a target arrangement. As a result, electrons can flow out of the confinement by following the field lines, enhancing the ionization of the Ar gas near the substrates. Due to the enhanced ionization of the Ar gas in the vicinity of the substrates, by applying a negative potential to the substrates, the substrates will be bombarded with Ar ions at the same time, which may be favorable to the deposited films. Type 1 and type 2 unbalanced magnetrons are the two varieties of unbalanced magnetrons. The center pole is the origin of all magnetic field lines in type 1 unbalanced magnetron. Because they come from annular sources, certain magnetic field lines in type 2 unbalanced magnetrons do not hit the central pole. The magnets can be positioned in geometry in unbalanced magnetron sputtering to restrict the plasma away from the wall chambers, resulting in a higher ion current density near the substrate.

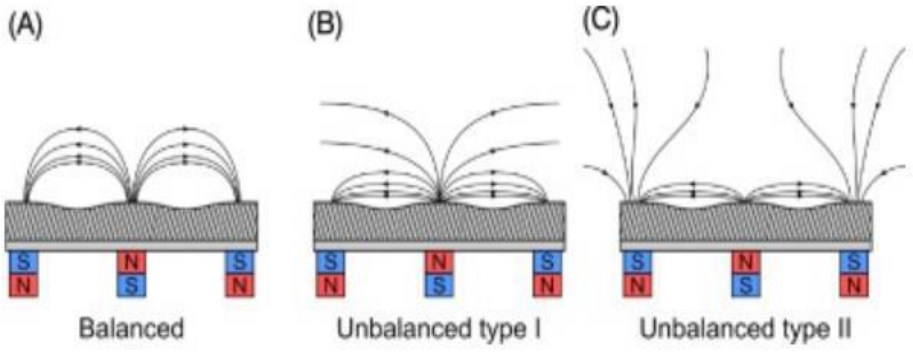

Figure 2.3. Schematic of balanced (a), type 1 unbalanced (b), and type 2 unbalanced (c) magnetron configurations[17].

Closed-field unbalanced magnetron sputtering [23] is the process used with this sort of magnet geometry. Different forms of magnetron sputtering are depicted in Figure 2.3.

TMD films suitable for tribological purposes have also been deposited using magnetron sputtering. In 2011, research used magnetron sputtering with a carbon target and a $WSe_2/MoS_2/WS_2$ target at the same time to successfully deposit a carbon alloyed TMD thin film [9]. More recently, research used closed-field unbalanced magnetron sputtering to deposit TMD thin film for tribological applications on a bigger scale. The work deposited $MoSe_2$ alloyed with carbon on Si wafers and steel cylinders using a semi-industrial deposition equipment [37].

The research stated above are only a few of many that demonstrate how the magnetron sputtering process may be used to create different TMD films on diverse substrates. Magnetron sputtering provides several benefits over other processes, making it perfect for the deposition of TMD films. TMD films are typically used in applications that needs high purity, rapid deposition, and vast area coverage, all of which are possible using magnetron sputtering. As a result, the approach will be used to deposit the work on film in this document.

2.4 Aluminium Galling

Tribology is important in both cold and hot metalworking processes because these processes demand a adequate level of friction to create the correct shaped components and to reduce tool wear for better process efficiency. Because friction and wear are very system-dependent, different hot metal forming techniques will produce distinct tribological phenomena, specific attention to the characteristics of the materials in contact, as well as the operating circumstances, is required. The spread of hot forming technology, notably in the automobile sector, is being driven by an increased interest in producing components built from high-performance materials.

Aluminium's light weight makes it a material of interest in a variety of industries, including the automobile industry. Because of their higher strength-to-weight ratio, the 6XXX and 7XXX aluminium series are commonly employed as structural steel component replacements. As a result, these alloys are excellent options for enabling future automobiles to comply with contemporary environmental energy consumption and passenger safety criteria.

As was previously established, aluminium is a naturally highly reactive substance that bonds easily with a wide variety of other elements. This is demonstrated in Figure 2.4 by the high solid solubility of aluminium in a variety of other metals [38]. This makes material transfer possible. The softer and more receptive aluminium is easily transferred to the harder mating tool, also referred to as galling, this makes material transfer possible. The two main causes of this

phenomenon are known origins: Mechanical interlocking of asperities and chemical bonding between the surfaces that interact [39]–[41].

Due to the spring back effect and the poor formability of high strength aluminum alloys at low temperatures, these alloys are frequently produced at elevated temperatures[42], [43]. For aluminium alloy components, hot forming and, in particular, hot stamping are typical manufacturing procedures. These procedures entail solubilization of the aluminum workpiece, followed by forming in the dies at elevated temperatures and a final quenching step within the dies[43].

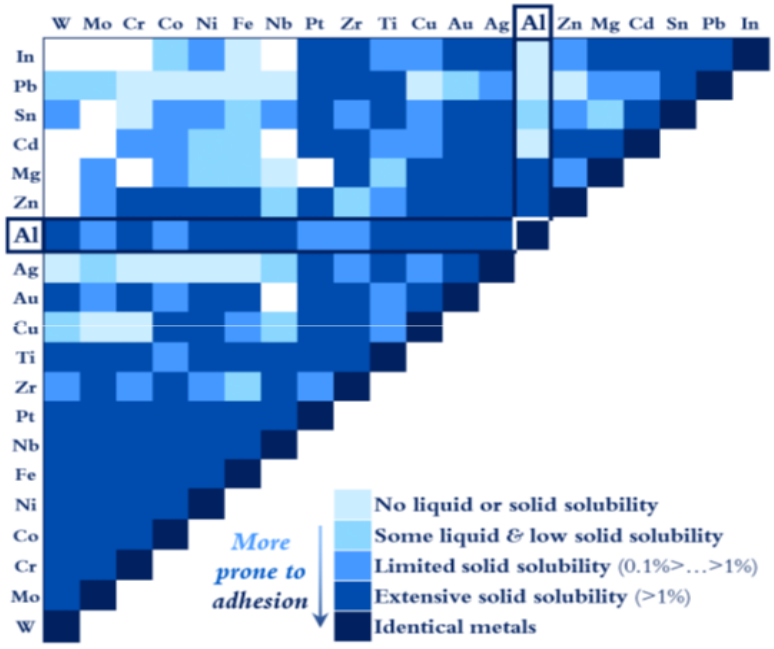

Figure 2.4. Relative mutual solubility of pairs of pure metals[38]

Elevated temperature forming of ductile and reactive materials like aluminium alloys results in challenging tribological phenomena including strong adhesion, also known as galling. This complicates the manufacturing process, especially given the time and cost constraints imposed by existing line production procedures [43]. When producing aluminium at elevated temperatures, essential wear mechanisms such as high adhesion and severe galling have been observed [44]–[46]. These wear processes have an impact on tool lifespan, surface quality, and mechanical qualities of manufactured components [39], [42], [47], [48]. As a result, direct forming costs (heating, tooling, lubrication, etc.) and maintenance costs (refurbishing, shutting down lines, etc.) increased significantly, reducing the appeal of employing aluminium for mass manufacturing.

High-temperature lubrication for the aluminium-steel contact has, however, many limitations. Common lubricants such as oils decompose and degrade when in contact with surfaces hotter than 200°C, making them unsuitable lubricants for hot forming [43]–[45].

For aluminium formation, solid lubricants such as graphite, MoS_2, and boron compounds have been investigated[49]–[51]. Graphite has excellent lubricity and thermal stability, making it ideal for hot forming [44]. However, because of health and environmental problems, as well as hygienic difficulties[46], [52], its usage is limited. In dry and vacuum circumstances, MoS_2 is reported to have exceptionally low friction. Its usage in the air at elevated temperatures, on the other hand, causes fast oxidation, which reduces its lubricity [44], [53].

It is clear that there is currently a paucity of understanding about efficient methods to inhibit the onset of aluminium transfer at elevated temperatures. The efficiency of high-temperature lubricants for friction and wear management in tribosystems including aluminium, particularly when combined with PVD coatings, is also unknown.

2.5 Research Gaps

From a technological and economic standpoint, the relevance and complexity of hot forming operations have sparked a rising interest in optimizing the tribology of the tool-workpiece interface. Because tribological interactions are known to be system-dependent, they must be optimized for a specific material combination under certain operating circumstances.

At room temperatures, the topography and chemical affinity of the tool's surface towards aluminium has a known effect on the aluminium-tool contact. Only a few studies have been conducted at high temperatures, and no global understanding of the tribological phenomena that occur in the contact has yet emerged.

As a result of the extreme material transfer that occurs during aluminium hot forming, wear and friction can increase dramatically. However, there is still a lack of knowledge about the mechanisms that cause galling at high temperatures and the effects it has on friction. Effective methods for controlling wear and friction are still being developed, and characterization of their tribological characteristics is even more limited.

Several research on the ability of different PVD and CVD coatings to reduce adhesion have been carried out. Even though some CVD coatings have shown to have strong anti-galling properties, the deposition approach requires high process temperatures. This will alter the microstructure and mechanical characteristics of the substrate, as well as create dimensional changes. PVD coatings, on the other hand, are a better fit since they are applied at lower temperatures.

Research based on the potentially promising anti-galling properties of aluminium were carried out with several types of coatings such as DLC coating but at elevated temperature DLC

coatings experience higher wear rates and more unstable friction than at room temperature due to graphitisation or dehydrogenation. Works related to Molybdenite, or MoS_2, provides a very low friction but at elevated temperature rapid oxidation in air at high temperature however adversely affects its lubricity.

There is currently a shortage of understanding about efficient methods to inhibit the onset of aluminium transfer at high temperatures. The efficiency of high temperature lubricants for friction and wear management in tribosystems including aluminium, particularly when combined with PVD coatings, is also unknown. Furthermore, there are few published studies on the effect of TMD coating on aluminium transfer at elevated temperatures. Tungsten-Sulphur-Carbon (W-S-C) coating perform extraordinarily well at high temperatures, with a maximum temperature of 400°C-450°C. It is believed that through this study a feasible solution to the issue of galling of aluminium at elevated temperature may be provided.

Thesis Aim

The goal of this research is to learn more about the tribological events that occur when aluminium slides across tool material at elevated temperatures. Specifically, the mechanics behind galling, as well as methods for limiting galling's onset and progression through the application of W-S-C coatings.

This proposed solution to tackle the galling of aluminium at elevated temperature by coating the surface with Tungsten-Sulfur-Carbon (W-S-C) coatings would be the primary looking point of this thesis.

However, to understand the phenomenon better and mitigate the adverse effect of galling of aluminium at elevated temperature it is essential to perform the following tasks and hence meet our objectives.

- Deposition of TMD-C- coatings with varied carbon content and a study of their fundamental Physico-chemical properties.
- Structural analysis of the coatings by the means of Raman spectroscopy and XRD.
- Mechanical characterization of the coatings by scratch and nanoindentation technique.
- Study of the tribological behavior of the coatings at room temperature and at elevated temperature testing against the aluminium counter bodies.
- Analysis of the wear mechanisms through post-test analysis of the wear scars using SEM/EDS, 3D profilometry, and Raman spectroscopy.
- Compare the performance of the coating for pure WS_2 coating and coating with varied carbon content.

CHAPTER 3

3. EXPERIMENTAL PROCEDURE

This chapter provides a detailed overview of the materials used for the specimens in the current work. There is also a full description of the different experimental procedures utilized, the experimental settings used, and the parameters used for each particular experimentation. The approaches used for various characterization procedures are described in detail.

3.1 Specimen Details

H11 tool steel was chosen as a substrate material for the application of the desired coating. H11 tool steel is a chromium-based steel alloy. The dimension of the rectangular plate had a length of 30mm, a width of 20mm, and a thickness of 4mm. For the preparation of the sample, we started with sandpaper grits ranging from P180 to P1200 to polish the surface to be coated. The samples were then polished to 1-micrometer diamond finish. This helps to remove any unwanted patterns or scratches that could affect the final result and also ensures the expected level of adhesion between the coating and the substrate. Table 3.1 shows the chemical composition of the substrate.

Chemical composition % by mass										
Element	C	Mn	Si	Cr	Mo	Ni	V	Cu	P	S
%	0.3-0.4	0.2-0.5	0.8-1.2	4.8-5.5	0.3	1.1-1.6	0.3-0.6	0.3	0.03	0.03

Table 3.1: Chemical composition of the substrate (weight %).

3.2 Surface Coating

For the coating of the prepared samples, a semi-industrial unit with four unbalanced magnetrons sputtering setup (Teer Coatings Ltd UDP 650/4) in a closed field arrangement was used having a dimension of 650mm in diameter and 650mm in length. For the deposition process, a vacuum below 3 x 10^{-4} Pa was maintained throughout by a rotary vane pump and a diffusion pump. An active inverted ionization gauge measures the ultimate vacuum pressure, while a capacitance manometer measures the deposition pressure. The entire deposition procedure took place in an Ar environment. Four targets (380 x 175 x 10 mm) were set vertically on the magnetrons inside the chamber walls. There were two graphite targets, one tungsten disulfide (WS_2) target, and one Cr (interlayer) target. To maintain a wider range of

carbon and uniformity two graphite targets were used with 99.99% purity. A schematic representation of the arrangements of the targets can be seen in Figure 3.1.

The substrates were sputter cleaned for 40 minutes before deposition utilizing a p-DC voltage of 600 V, a frequency of 250 kHz, and a reverse time of 1.6 µs. The targets were cleaned for a period of 20 minutes, while the targets were being cleaned appropriate shielding was placed in front of them to ensure that the targets are not cross-contaminated. However, before deposition of any alloyed coating, a Cr interlayer was applied, Cr interlayer significantly improves the adhesion between the substrate and coating as discussed previously. After the deposition of Cr interlayer, a gradient of Cr/TMD-C was deposited by slowly reducing the power supplied to the Cr target while increasing the power supply of the C and WS_2 targets. The application of gradient interlayer ensures a more gradual change in composition rather than a sudden change in the composition.

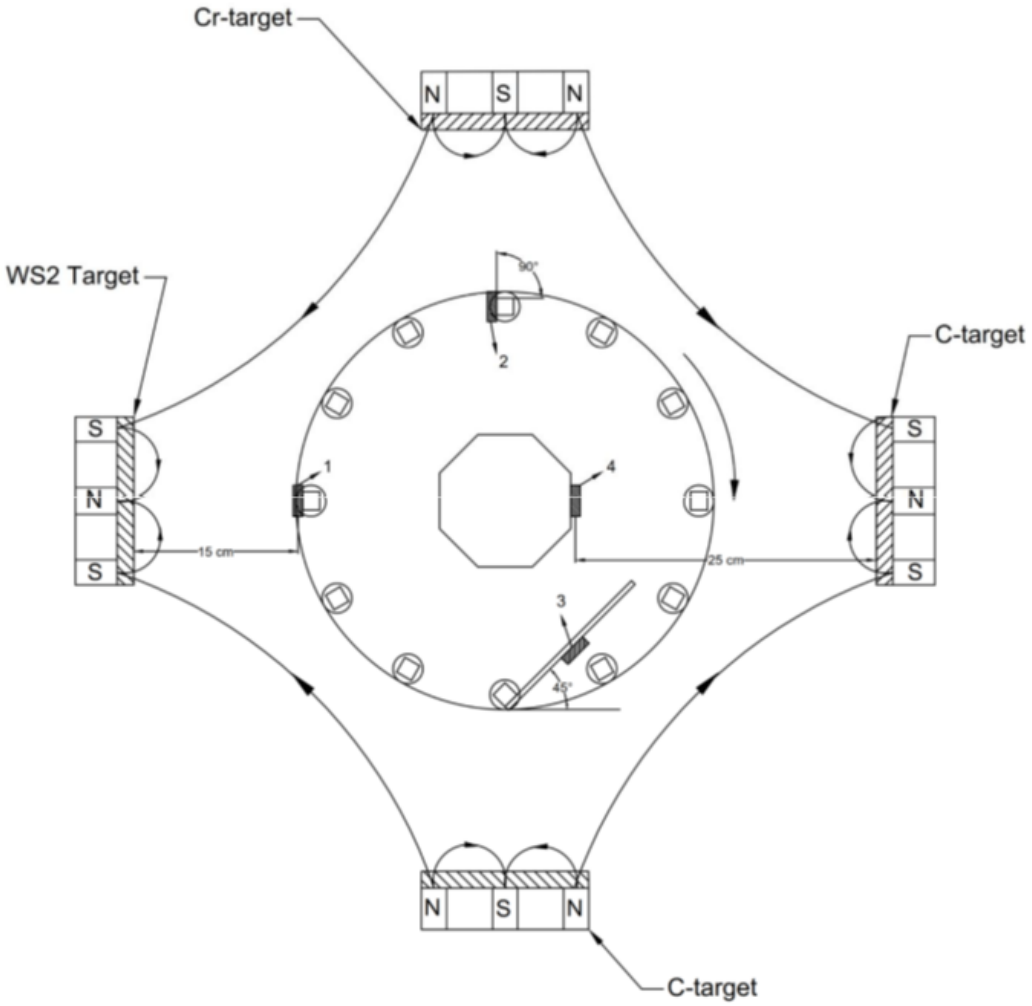

Figure 3.1: Schematic representation of the magnetron sputtering unit with target arrangements.

Figure 3.2: Deposition unit setup coatings.

Three different recipes were used for coating the polished H11 tool steel samples varying the carbon content. Table 3.2 shows the variation of C content and the used power for the desired coating.

Name	Power on C Target	Power on WS_2 Target	Carbon %	Biased Voltage
$WS_2$50V	-	1000W	6.7%	50V
WSC1010	500W on each	1000W	27.4%	-
WSC1016	800W on each	1000W	35.3%	-

Table 3.2: Variation of Carbon content according to supplied power.

The coating will further be referred to as $WS_2$50V, WSC1010, and WSC1016 from now onwards. The chemical composition was varied by varying the power density applied to the graphite targets and setting the power density to the WS_2 target fixed at 2.1 W/cm^2. Vuchkov et al. issued a paper with a detailed description of how the coatings were applied and all the

parameters that were used [54], a similar coating approach was followed for our project as well.

3.3 Characterization technique of the coating

3.3.1 Chemical Composition

The chemical composition of the deposited coatings was ensured by the wavelength dispersive spectroscopy detector (WDS) that was coupled with a field emission scanning electron microscope (FESEM, Zeiss Merlin). The analysis was carried out using Oxford Instruments' INCA software at the IPN facilities. 15 kV was used as the accelerating voltage.

3.3.2 Morphology

In order to understand the morphological features of the coating field emission scanning electron microscope was used. Typically, a magnification of 25k-50kx was used. However, to have a clear idea about the thickness, cross-sectional images of coatings deposited on silicon wafers were analyzed. To have a better understanding of the coating, secondary electron imaging was performed with an accelerating voltage of 2 kV. FESEM also was also used to analyze the wear track and the generated debris to identify the extent of materials transfer from the aluminum ball and also the nature of the wear.

Figure 3.3: The SEM instrument equipped with WDS detector used for studying morphology and chemical analysis of the film.

3.3.3 Optical Microscopy

3D Optical microscopy (Alicona Infinite Focus^{TM} G4) was used very often to study the wear scar of the aluminium ball after the tribological tests were performed and to construct the 3D image of the wear tracks. This gives an idea about the extent to which the aluminium ball was damaged. A scan of the aluminium ball was taken after each test to compare the wear at different temperatures along with the wear of the coated samples as well as the uncoated sample.

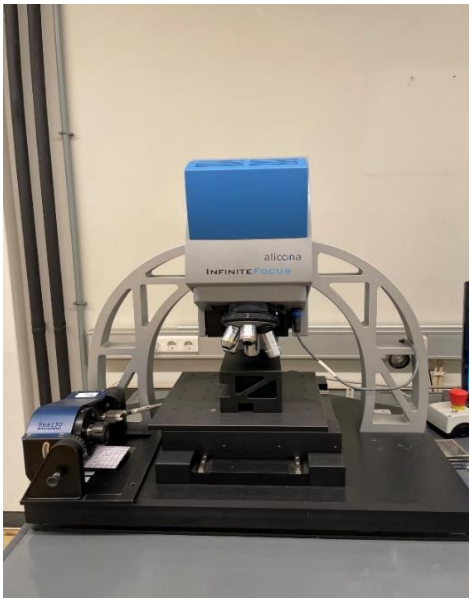

Figure 3.4: The optical microscope used in the analysis of scar.

3.3.4 Crystal Structure

To study the crystallographic structure of the sample X-ray Diffraction was used. In our case, Malvern Panalytical X'Pert MRD diffractometer was used as seen on figure 3.4

Figure 3.5: XRD setup for the experiment.

The angle of incidence was varied from 5° to 90° (2θ) with a step size was 0.025°, and Co Kα (λ=1.5406 Å). Obtained results were compared with that of the standards to identify the crystal structure of the deposited coating.

3.3.5 Adhesion

To understand the adhesion between the substrate and the coating scratch test was performed on a multifunctional tribometer MFT-5000 from RTEC instruments (scratch test module). Scratch test was performed on all the coated samples multiple times. A Rockwell C-type indenter with a diameter of 200 micrometers was used for the test. In our experiment rate of horizontal displacement was 0.16 mm/min and with a loading rate of 100 N/min. Loading was varied from 2N to 70N gradually. Figure 3.5 shows the typical representation of the arrangement for the scratch test.

Though the fundamental adhesion strength of the link between the coating and the substrate is not measured by the test method. Rather, the test method provides an engineering assessment of a coating-substrate system's practical (extrinsic) adhesion strength, which is determined by the complex interaction of test parameters (stylus properties and geometry, loading rate, displacement rate, and so on) and coating/substrate properties (hardness, fracture strength, modulus of elasticity, damage mechanisms, microstructure, flaw population, surface roughness, and so on).

By carefully identifying the positions of the critical loads (L_{C1} , $L_{C2,}$ and L_{C3}) by the optical microscope adhesion of the coating was quantified. L_{C1} denotes the occurrence of first cracks also called chevron marks on the initial portion of the wear track. L_{C2} gives an idea about position of initiation of chipping which in turns gives the load at which it occurs. And finally, L_{C3} where the coating starts to spall, and more than half of the wear track is exposed.

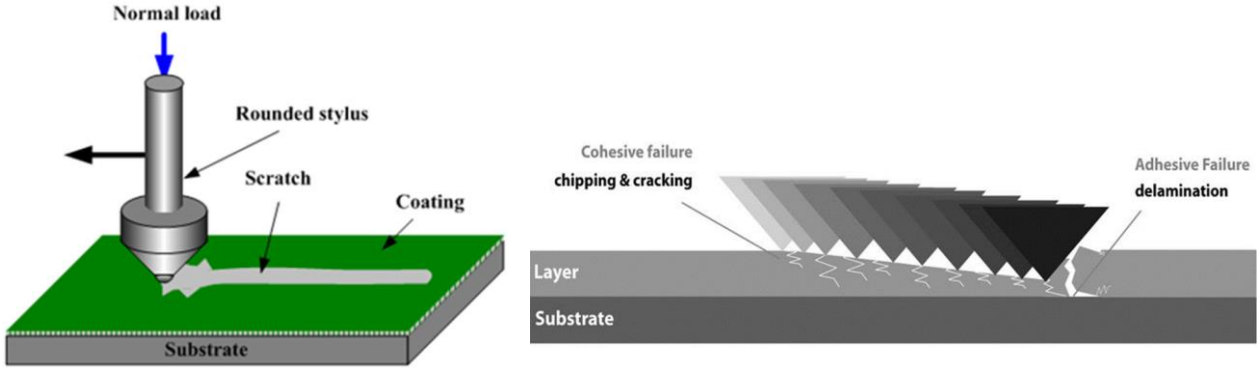

Figure 3.6: Figure 3.6: (a)Schematic representation of the scratch test setup (b)Principle of scratch test[71]

3.3.6 Mechanical Properties

Hardness and the Youngs modulus of the samples were assessed by nanoindentation with a Berkovich pyramid diamond indenter. Multiple indentations were made on the same sample and calculated the value of hardness. The hardness values utilized in this study were determined by averaging 16 such measurements made at two separate places on coatings applied to steel substrates (a total of 32 measurements were used for statistical analysis). The Oliver-Pharr approach is employed to obtain the findings. At room temperature (25 °C) and around 45 percent humidity, measurements were made on the free surface of each sample. 7 to 10 percent of the coating thickness was indented on average. Tests were carried out for a load of 3 mN.

3.3.7 Tribological Analysis

At different temperatures, all of the deposited coatings were submitted to various tribological tests to understand the frictional behavior by a reciprocating ball on disc experiment. RTEC Instruments' multifunctioning tribometer (MFT 5000) was extensively used for the tribological analysis. The experimental setup for tribological experiments is shown in Figure 3.7.

A constant normal load of 5N was applied throughout with a frequency of 5Hz and was carried out for 5000 cycles with a stroke length of 6mm. Table 3.3 summarizes the conditions and parameters used while carrying out the experiments. As we are studying the galling of aluminum at elevated temperatures hence aluminium ball with a diameter of 10 mm was used as a counter body for the tribological tests, Figure 3.8 shows the arrangement of the aluminium ball and the holder.

Figure 3.7: Tribological test setup, multifunctioning tribometer.

Tribological tests at elevated temperatures were performed in the same tribometer using the high-temperature module. The tests were carried out at RT (25 °C), 200°C, and 400°C for all the samples. However, tribological tests for uncoated surfaces could not be conducted for full cycles at elevated temperatures due to excessive friction and material transfer. Other parameters, such as humidity (RH ~ 35 – 45%), and pressure were not manipulated, which stayed relatively constant throughout the testing

Test Parameter	
Load [N]	5N
Duration [Number of cycles]	5000
Counter body	Aluminium Ball
Speed [m/s]	0.1 m/s
Stroke[mm]	6
Temperature	RT, 200°C, 400°C
Pressure	Atmospheric

Table 3.3: Parameters for the tribological tests.

The specimen and aluminium ball were both sonicated in ethanol for ten minutes each prior to the test. For every coating two tests were performed at each temperature to confirm the reproducibility of the obtained results. The 3D optical profilometer attached to the tribometer was used to take the wear profiles of the coated samples. Gwyddion software was used to analyze the wear profiles and extract the 2D profile of the scar. And later on, using the Origin software wear profiles were plotted to calculate the wear of the track of each sample.

Figure 3.8: Aluminium Ball used as a counter body on the holder.

CHAPTER 4

4. RESULTS AND DISCUSSION

4.1 Chemical composition, morphology, and structure

The results of the WDS analysis of the coating are shown in the table 3.4. Variation of thickness for different coating is presented on the table as well as the chemical composition. Film thickness for the WSC1016 coating with the highest percentage of carbon is the lowest and WSC 1010 has the thickest film of all. Another notable characteristic that can be observed from the table is that S/W ratio is decreasing with the increase of carbon % in the deposited films. The presence of chromium is also noticed that is from the deposited interlayer. In our deposited sample S/W ratio varied from 1.34 – 1.50, this is particularly an important parameter as it can influence the tribological behavior of the coating[55]. A similar kind of S/W ratio was also obtained by Vuchkov et al. [56] using the similar deposition unit and setup.

However, in all the coating samples presence of Oxygen can be seen, this is due to the residual oxygen present in the sample, and also could be because of the contamination of the targets. The highest amount of oxygen present is around 9% on the $WS_2$50V sample and gradually decreases to around 3%. The chemical events that occur in the chamber during the deposition can be linked to the decrease in O in these films. Because active C species are present in the atmosphere, they can combine with O atoms to generate CO or CO_2 molecules, which are then pumped out of the chamber. Furthermore, C alloying promotes coating density, minimizing the specific area exposure to the environment greatly [19].

As expected, increasing the power supplied to the graphite targets, the amount of carbon content increased in the deposited sample. The ratio of the power supplied to the graphite targets to WS_2 targets varies from 0 to 1.6. For the power ratio of 1.6, the highest quantity of carbon is present on the film and also the least thickness. A gradual decrease in the amount of S is observed, the low S/W ratio is most likely related to the scattering behavior difference as well as the bombardment with backscattered Ar neutrals. During their journey towards the substrates, the sputtered species C, S, and W will spread in various ways. Collisions with the Ar gas in the chamber will cause the lighter elements, C and S, to be deflected to a greater extent. The W atoms, which are significantly heavier, will follow a straight path to the substrates. A reduction in the Sulphur content can be observed from the table. This could possibly be for many reasons; one such could be preferential resputtering of Sulphur atoms caused by the Ar neutrals [57]. Also, due to the higher mass of tungsten than Sulphur by re-sputtering of S by argon ions is believed to have caused a reduction in S content in comparison to W.

Sample type	Power ratio [P_c/P_w]	Chemical Composition (at. %)				S/W ratio	Thickness [µm]
		C	S	W	O		
$WS_2$50V	0.0	6.5 ± 0.1	50.7 ± 0.4	33.7 ± 0.1	9.1 ± 0.2	1.50	1.5
WSC1010	1.0	27.4 ± 0.4	39.1 ± 0.3	29.1 ± 0.1	4.4 ± 0.1	1.34	1.5
WSC1016	1.6	35.3 ± 0.2	36.3 ± 0.1	25.1 ± 0.3	3.3 ± 0.2	1.45	1.3

Table 4.1: Chemical composition of the deposited coatings.

The chemical composition of TMD coatings produced by magnetron sputtering processes is mostly governed by two processes [58]:

i) Heterogeneous scattering behavior of sputtered species.

ii) Preferential re-sputtering of the chalcogen atom due to energetic particle bombardment of the developing layer during deposition.

Figure 4.2 shows the SEM micrographs of the cross-sections of the deposited films. From the cross-sectional micrographs, it can be seen that with the increase of the carbon content compactness of the coating has increased. Clear presence of the Cr interlayer can be identified from the micrographs. For $WS_2$50V a columnar growth of the coating can be noticed, however, this is not visible for the increased carbon content of the coatings. There is also a clear presence of porosity in $WS_2$50V coating, however, a reduction in porosity can be observed with the increase of carbon content as suggested by Cavaleiro et al [59]. Coating with the highest S/W ratio and lowest carbon content shows the presence of the previously mentioned columnar and porous structure. By the increase of carbon content on the coating the structure tends to become more featureless. The thickness of the film varies from 1.28 – 1.53 µm, WSC1016 having the minimum thickness with highest carbon content.

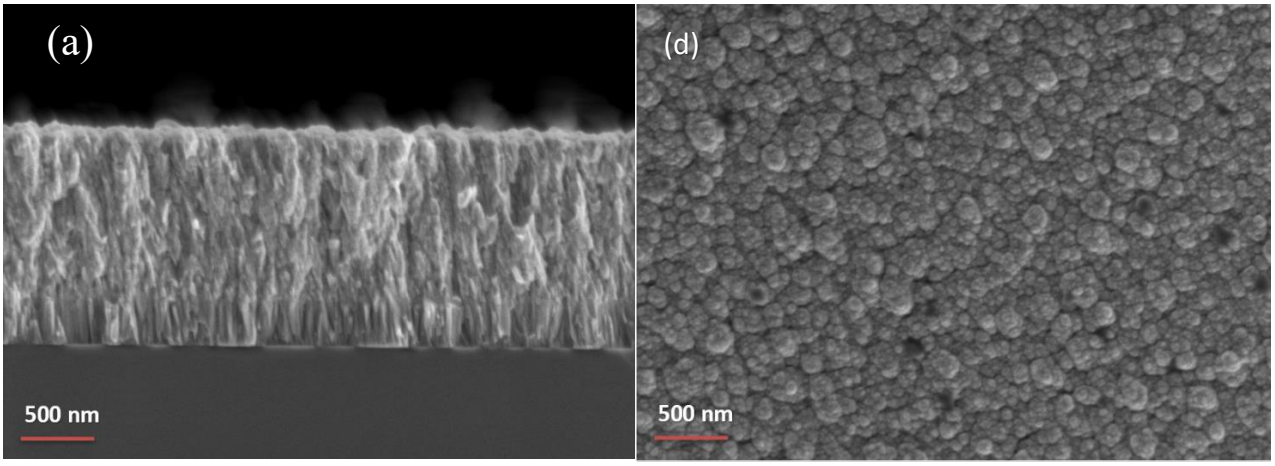

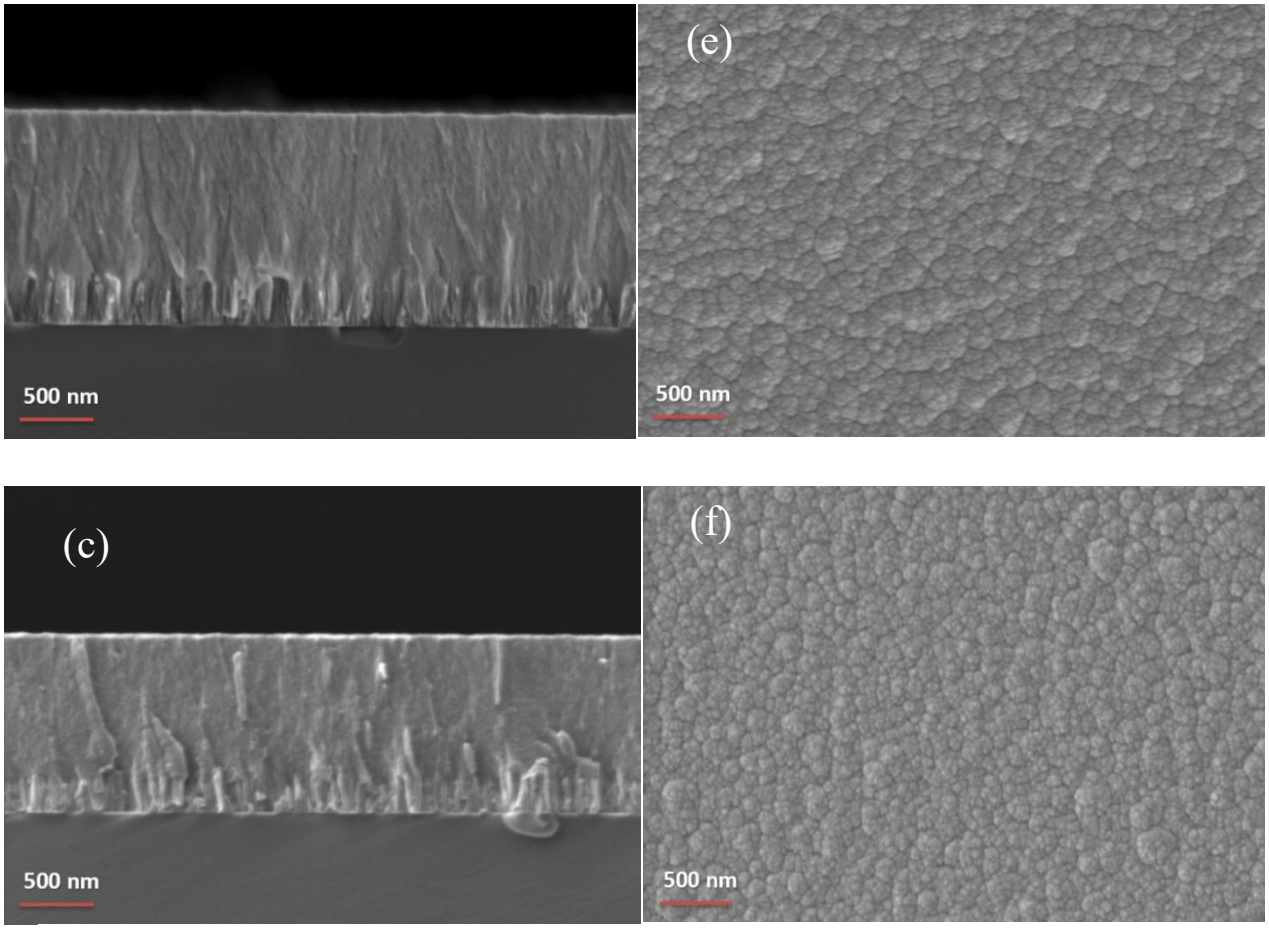

Figure 4.1 : Cross-sectional SEM micrographs of: (a) $WS_2$50V; (b) WSC1010; (c) WSC1016; and their respective top surface morphology of (d) $WS_2$50V; (e) WSC1010; (f) WSC1016.

From the top view of the micrographs, as shown in Figure 4.2 (d), (e), (f) the presence of droplets on the surface coatings caused by arc discharge during the deposition process which is a characteristic of sputtering process. The typical cauliflower structure of the film is observed. This is rather an expected structure for the coatings deposited by a magnetron sputtering unit. Morphologies shown in Figure 4.1 agrees with that of the findings of Vuchkov et al.[56].

The atoms remain in their arriving locations under low mobility circumstances. As the film thickens, adatoms will be caught preferentially at the tops of the hills, resulting in rough surfaces and the development of columnar structures as a result. The porous shape has been attributed to films forming in unstable growth conditions due to limited surface diffusion[60]. Pure TMD coatings, especially WS coatings, typically have a sponge-like morphology with significantly increased porosity. The low S/W ratio of these films, which is known to cause coatings compactness.

Figure 4.3 shows the XRD diffractograms of the deposited films. Typical peaks for sputtered WS_2 films indexed as (100) and (110) are present. For the deposition of WS_2 films without the presence of carbon, type I structure (peak (10L) with L=0,1,2, 3 for $2\theta \approx 40^o$ and (110) for $2\theta \approx 72\ ^o$[61]. The characterized broad peaks 35^o to 45^o, this range's broad peak might have peaks connected to the WS_2 and WC planes. With a tail toward higher angles signifying the turbostratic stacking of (10L) WS_2 planes with L having values of 1, 2, and 3 [62], the peak frequently seen in this range is associated with the (100) plane of WS_2 at $2\theta = 33°$. On the other hand, in addition to a WC1-x (111) peak at $2\theta = 38°$ and a W_2C (002) plane at 39°, there is also a W_2C (100) peak at $2\theta = 34.5°$. The interpretation of the diffractogram is challenging since this region contains both tungsten disulfide and tungsten carbide peaks. But even if they are there, the WS_2 and WC crystals are too tiny to be seen by XRD. As the percentage of carbon increases, the sharper peaks become broader. The weak bonds between the sandwich layers in WS_2 generate turbostratic stacking, which causes rotational and/or translational disorder around the c axis [63], [64].

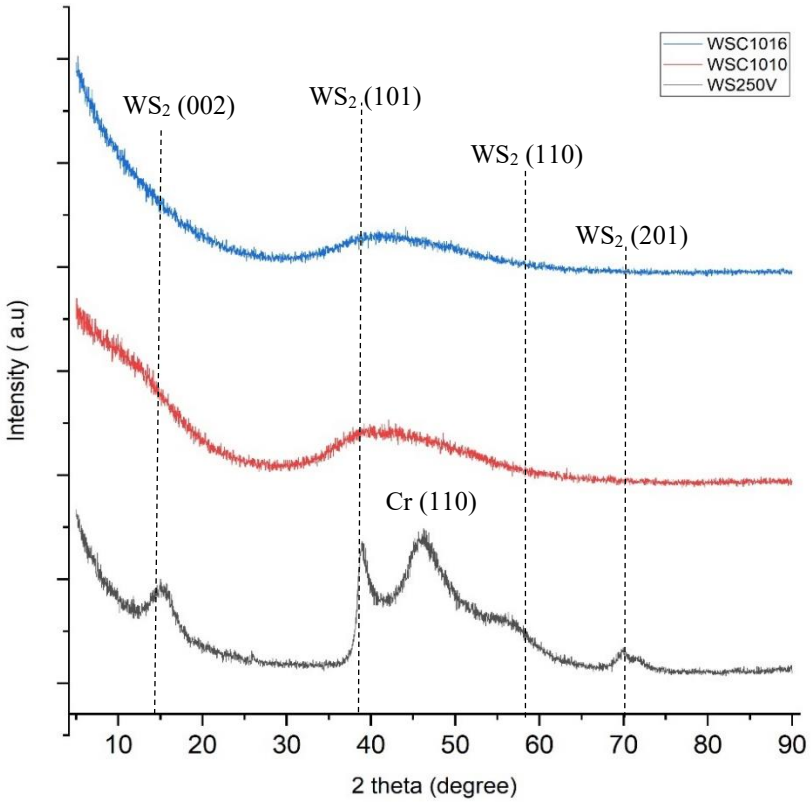

Figure 4.2 : XRD diffractograms of W-S-C films

Different peak positions, intensities, and broadening were seen depending on the alloying content. Amorphous materials only produce broad scattering features because they lack a periodic array with long-range atomic order. As a result, the diffraction from them lacks distinct Bragg peaks [65].

The loss of crystallinity is enhanced when carbon is added to the films. Other phrases, such as W–C compounds, can be found, as has been observed in a previous investigation [59]. These peaks become broader with decreasing crystalline domain size as the C content of the alloyed coatings increases. Only one very broad peak can be seen in these films in the same locations as the (10L) line of the WS_2 phase. These films have an amorphous structure, regardless of the C concentration.

The C-alloyed coatings have broad characteristics at the same peak positions, and as a result, they are comprised of even smaller clusters with restricted long-range order. The enhanced possibilities for the atoms to diffuse on arrival to the substrate can be linked to the difference in crystallinity between pure and alloyed coatings.

4.2 Hardness behavior and adhesion

4.2.1 Hardness

Table 3.5 summarizes the obtained hardness and reduced modulus of the coated samples from the nanoindentation test. Figure 4.3 (a) shows the variation of hardness with varying the carbon content in the coating and Figure 4.3(b) shows the reduced modulus of the deposited films. Despite keeping the columnar shape, the films alloyed with biased voltage shows a rise in hardness when compared to the pure W–S film, as found by Sundberg et al. [63] to be around 2GPa. The alteration of the morphology and structure is primarily responsible for this behavior. The removal of the characteristic pores of the columnar morphology increases the compactness and density of the films while also allowing the structure to grow with a significant reduction in grain size [66].

$WS_2$50V exhibits the lowest hardness of 2.8GPa whereas WSC1010 and WSC1016 show a similar hardness of around 5GPa. A similar trend in the value for reduced modulus is also observed in WSC1016 and WSC1010 having a similar value of 90GPa. The elemental composition of the coatings can influence their hardness. Specifically, as the overall S/W ratio is dropped, the coatings' hardness increases. WSC1010 has the highest value for hardness and has the lowest S/W ratio of 1.35 and $WS_2$50V is the softest with the highest value for the S/W ratio of 1.51. Because the S/W ratio is low, more tungsten is present for the development of hard tungsten carbide inclusions. The maximum hardness achieved for the WSC1016 coating might be due to increased concentrations of tungsten carbide phases.

Coating	Hardness (GPa)	Reduced Modulus (GPa)
$WS_2$50V	2.8±0.3	69.4±3.8
WSC1010	5.8±0.2	89.9±1.9

WSC1016	5.6±0.3	90.9±2.8

Table 4.2: Mechanical properties of the coating.

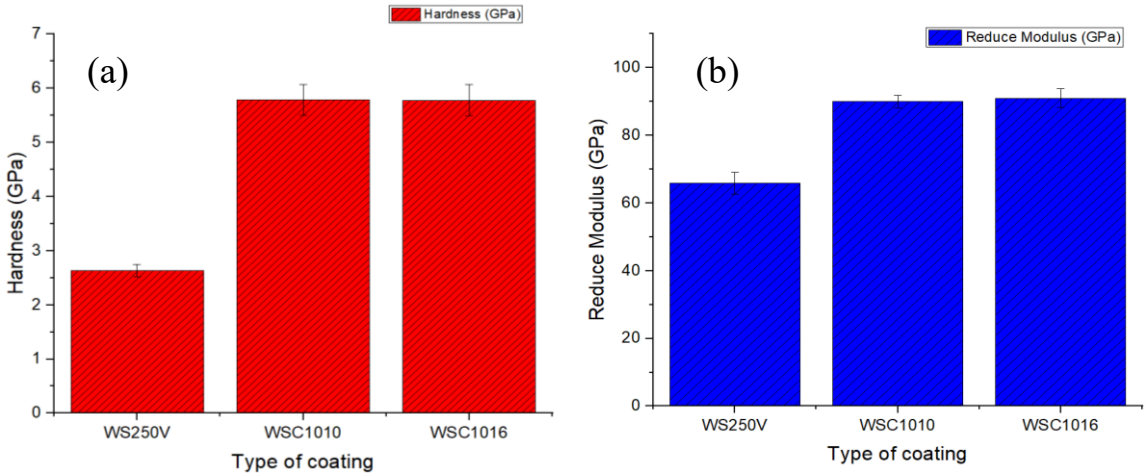

Figure 4.3: a) Hardness and b) Reduced modulus of the coatings

The greater S/W ratio for $WS_2$50V suggests the presence of a softer WS_2 phase, which reflects the observed hardness drop. Furthermore, enhanced adatom mobility might result in increased density of the morphology when the growing films are bombarded with Ar neutrals at a greater intensity [67].

4.2.2 Adhesion

Figure 4.5 shows the optical image of the wear scar after the scratch test. Multiple tests were carried out on the sample and observed characteristics and measured values of corresponding critical loads (Lc) were similar. For the scratch test loads were varied from 2N to a maximum value of 70N at a rate of 10 N/mm. From the optical micrographs, corresponding values of the critical loads were measured, table 3.6 summarizes the critical loads of the deposited films.

Coating	Critical load (L_{c1}), [N]	Critical load (L_{c2}), [N]
$WS_2$50V	-	19.4
WSC1010	5.3	26.5
WSC1016	6.2	25.8

Table 4.3: Critical loads (Lc) of the coatings

The earliest formation of cracks on the border of the scratch scar correlates to L_{c1}. The L_{c2} critical load relates to the initial delamination (chipping) that occurs on the sides of the scratch scar, whereas the L_{c3} critical load refers to the load at which the coating is peeled from the surface[68]. For $WS_2$50V Lc1 was not detected but L_{c2} was found to be around 19N, the lowest

of the three coatings tested. For WSC1010 Lc1 was visible at around 5N and Lc2 at about 26 which is higher than that of the value found in $WS_2$50V with the lowest carbon content. For WSC1016 Lc1 was about 6N and Lc2 was found to be at around 25N, very much comparable with the value of WSC1010. However, for either of the coatings tested Lc3 could not be observed.

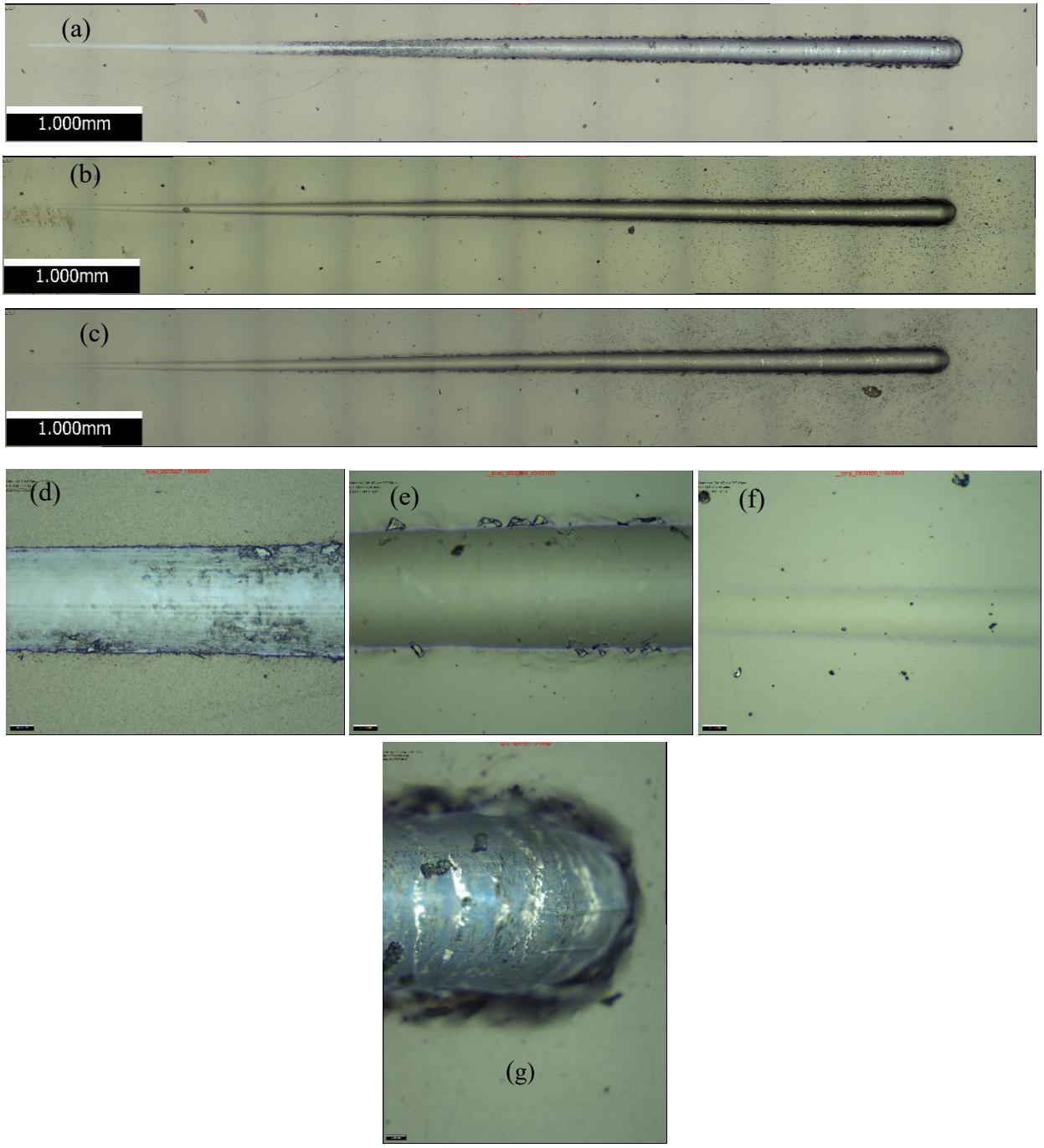

Figure 4.4 : Scratch scars optical micrographs: (a) $WS_2$50V; (b) WSC1010; (c) WSC1016; (d) Lc2 detail of $WS_2$50V; (e) Lc2 detail of WSC1010 (f) Lc1 detail of WSC1016 (g) end of scar detail for $WS_2$50V.

For $WS_2$50V initial formation of the chip was earlier than the other two. This could be described as due to the less compact and porous morphology of the coating. In terms of fracture initiation and propagation, columnar boundaries are unfavorable, making the films more prone to spallation, which is clearly the case for $WS_2$50V coating. On the other hand, WSC1010 and WSC1016 have a more compact and featureless morphology resulting in more resistance to spallation and crack formation. The results correlates to the finding of Mutafov et al. [69].

4.3 Tribological Properties

To understand the tribological behavior of the coatings, samples were subjected to the reciprocating ball-on disc test. And the corresponding values for the coefficient of friction, wear rate, and wear track analysis was carried out.

Figure 4.6 represents the evolution of the coefficient of friction of the coatings at different temperatures. Figure 4.6 (a) shows the plot of COF for the uncoated H11 tool steel at RT, 200°C, and 400°C. At room temperature the uncoated sample shows a very short running-in period, however, the friction drops to around 0.57 after around 10s into the experiment. At 200°C the sample shows the variation of COF is higher than at the RT eventually drops to around 0.60 before suddenly increasing after 220s. This indicates the transfer of aluminium causing an abrupt change in the quantity of COF. However, at 400°C the COF increased significantly and due to excessive wear on both the ball and uncoated sample, the test could not be carried out further. It should be noted at 400°C the material transfer from the ball increased significantly. From Figure 4.8 (b), (c) we can clearly see the transfer of material from the ball to the disc at 200°C and 400°C. Generated profile of the wear tracks also shows the significant transfer of material from the ball.

Figure 4.6 (b) shows the plot of COF for $WS_2$50V coating at different temperatures. At RT the fluctuations of COF are much higher, and the value of COF falls over time suggesting the formation of the TMD tribolayer to reduce the friction down to 0.16. A significant drop in COF is seen comparing to the COF of uncoated sample. Upon examining the wear micrographs of the sample does not show any noticeable damage to the surface nor any transferred materials from the aluminium ball. For the experiment at 200°C, a long running in time can be seen , and the COF fluctuates around 0.2. However, interestingly COF keeps dropping over the time to reach a value of as low as 0.14. A similar trend in dropping of COF is also observed for experiment at 400°C but the COF is lower than the observed value at RT and 200°C. However, initially the COF reaches a stable value of 0.14 before gradually reducing after 250s. This justifies the previously discussed quality of TMD to perform better at elevated temperature due to the removal of moisture. However, unlike the uncoated sample evidence of transferred material from the ball could not be found even at elevated temperature.

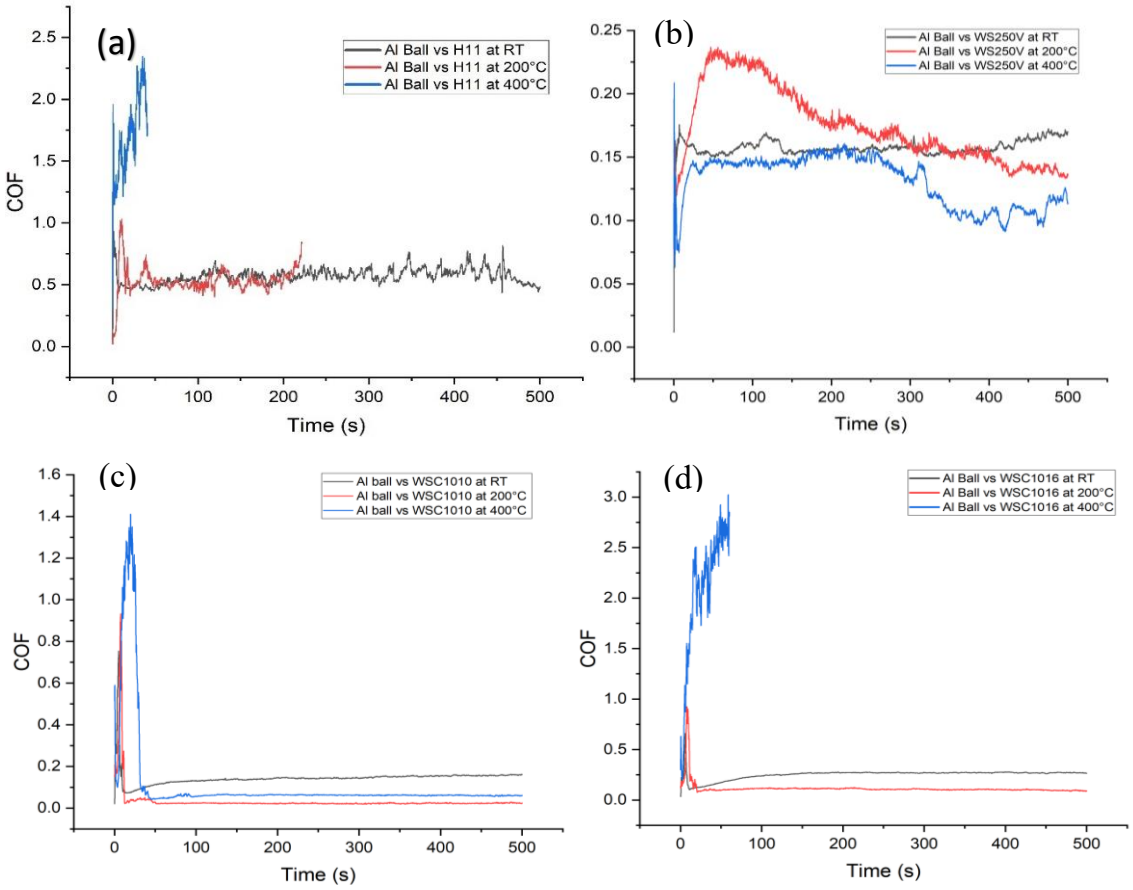

Figure 4.5: Tribological properties of selected coatings, coefficient of friction: (a)Uncoated sample; (b) $WS_2$50V; (c) WSC1010; (d) WSC1016.

Figure 4.6 (c) shows the plot of COF variation for WSC1010 coating at different temperatures. Compared to $WS_2$50V and uncoated H11 tool steel WSC1010 has a much shorter running-in period. COF reaches a stable value of 0.15 at RT, 0.02 at 200°C, and 0.06 at 400°C. WSC1010 coating has the least COF value at 200°C in comparison with the other coating. WSC1010 coating shows an excellent stable COF in comparison to the other coatings. Such values of COF could be lead us to say that the friction is partially controlled by WS_2 phase. 3D optical images of the wear tracks show no sign of coating delamination or transfer of materials from the aluminium ball.

On the other hand, for WSC1016 running in and period was similar to that of WSC1010. However, COF at RT settles down at 0.27, and 0.11 at 200°C. Obtained values of COF are higher than that observed for WSC1010 coating with 27.4 at. % of carbon, this could mean the presence of harder tribo material leading to an increase in COF. Though at 400°C COF was much higher and the experiment could not be carried out further. From the 3D optical images of the wear track, it can be concluded WSC1016 shows integrity until 200°C, significant quantity of ball materials can be seen to be transferred.

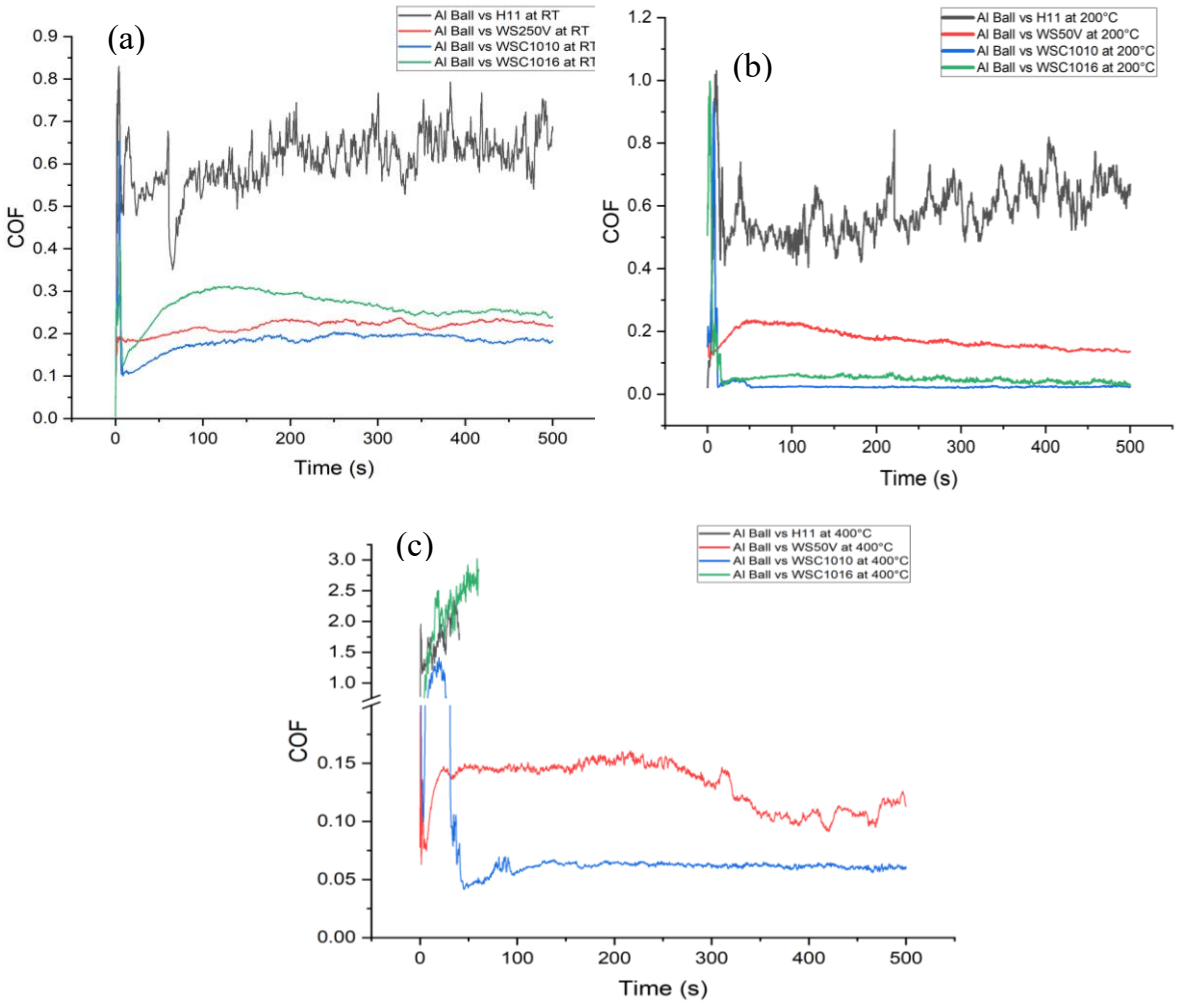

Figure 4.6: Tribological properties of selected coatings, coefficient of friction: (a) RT; (b) 200°C; (c) 400°C.

Figure 4.6 shows the plot of comparison of the performance of the coated samples. As can be seen from the graph at room temperature WSC1010 has the least value of COF followed by WSC250, WSC1016, and the uncoated sample. Similarly at 200°C WSC1010 attains the lowest COF after the running-in period. But in this case, WSC1016 shows a lower average COF than $WS_2$50V. However, WSC1010 continued to have the least value of COF even at 400°C.

Figure 4.7, 4.8 shows the 3D image of the wear tracks taken after the test. At room temperature apart from the uncoated H11 tool steel, all other coated sample shows minimal wear. From the micrograph presence of any transferred aluminum could not be identified at RT as well. However, at 200°C sign of materials transfer could be seen on the uncoated sample. Apart from the uncoated steel presence of any of galled aluminium is not visible on any of the coated samples. The optical micrograph of the wear scar does not indicate any delamination of

the coating at 200°C. However, at 400°C large quantity of material from the ball is transferred apart from WSC1010 coating.

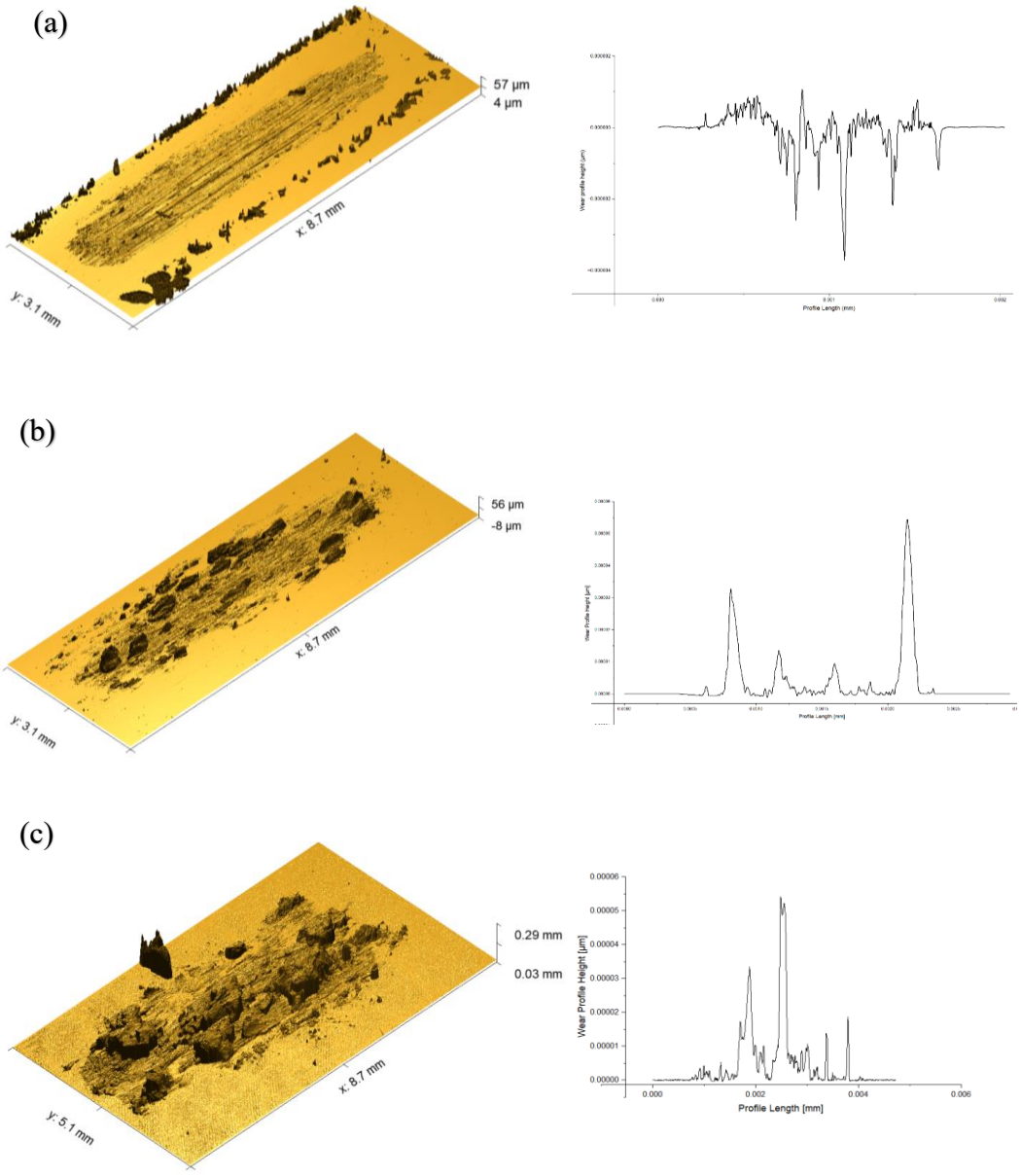

Figure 4.7: 3D images of the uncoated samples wear track at (a)RT; (b) 200°C*; (c)* 400°C

In summary it can be said that WSC1010 outperforms all other coatings in terms of COF both at RT and elevated temperature. Also, WSC1010 coating reduced transfer of ball material, aluminium to the wear track. Its good performance could be linked with the compact structure and optimal amount of carbon content on the coating.

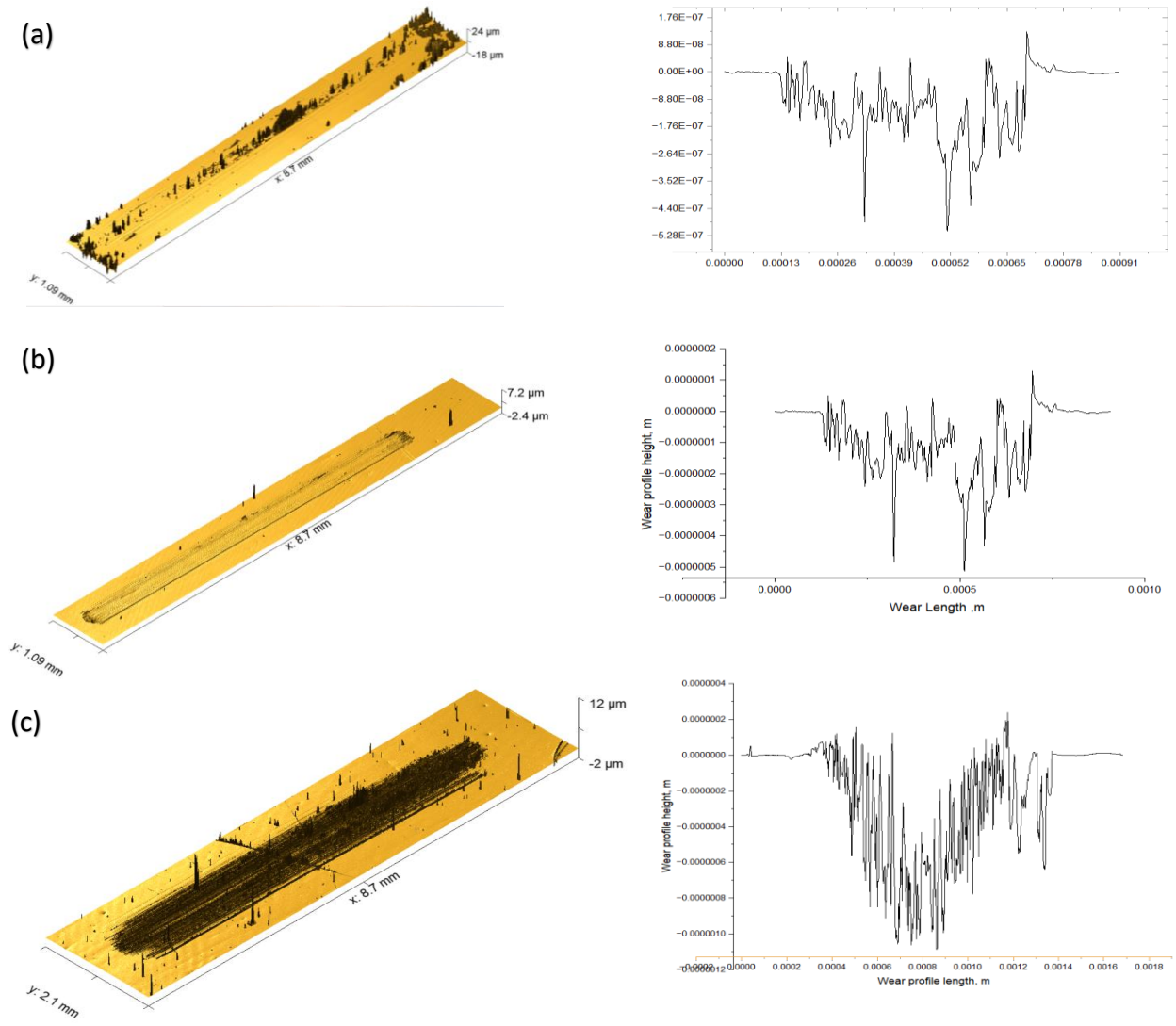

Figure 4.8: 3D images of the $WS_2$50V coated wear track at (a)RT; (b) 200°C*; (c)* 400°C

Measuring the width of the wear it is found that performing the tests at elevated temperature leads to increase in width of the wear track. However, increase in depth of the wear track at elevated temperature is also noticed. For the uncoated steel width as well as the depth of the wear track is found to be maximum.

Figure 4.9 shows the optical images of the aluminium ball after performing the test. Severe damages to the ball were observed for the tests which were performed at elevated temperature. The damage to the aluminium ball is also caused by the comparatively harder coating with higher carbon content.

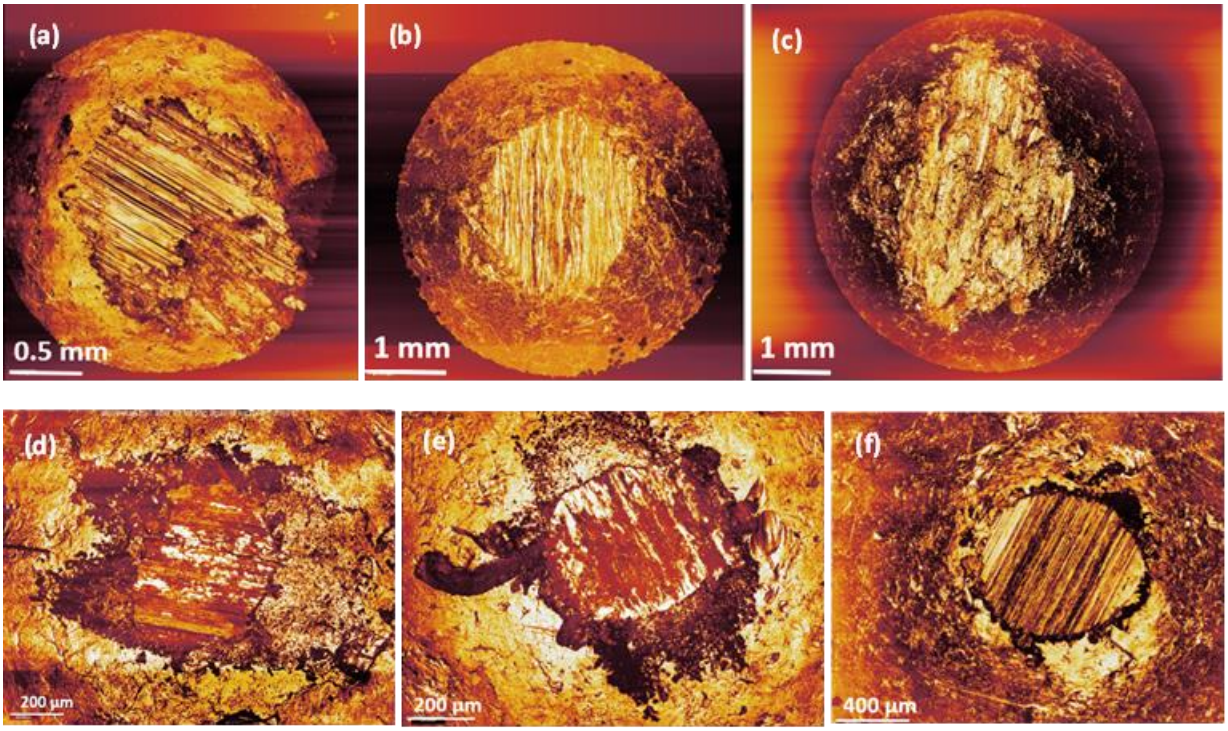

Figure 4.9: Optical Image of the aluminium ball vs uncoated steel at (a) RT; (b) 200°C*; (c)* 400°C ; and vs $WS_2$50V at *at (d) RT; (e)* 200°C*; (f)* 400°C ;

Previously Polcar et al. [68] studied the tribological behavior of W-S-C coating at elevated temperature varying the carbon content from 29 up to 70 at. %. He also found that wear rate at elevated temperature also increased significantly. He obtained a wear rate of around $2x10^{-6}$ (mm^3/Nm) for W-S-C coating sliding against 100Cr6 balls at RT and lower wear rate at 200°C.

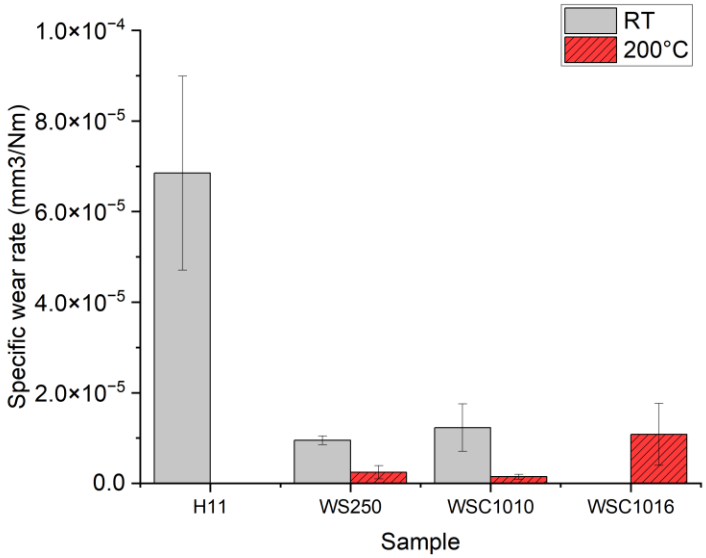

Figure 4.10: Specific wear rate of the uncoated and coated samples at RT and 200°C

4.10 shows the wear rate of the samples at RT and elevated temperature. The material transfer rate significantly dropped at elevated temperatures compared to the wear rates at RT for the coated samples. This is strengthened by the idea of removing the moisture at elevated temperature and forming tribolayer leading to the decline in COF which in turn result in a lower wear rate. Comparing the wear rate of all the samples, as suggested by the COF, the wear rate at 400°C is higher. However, the wear rate of the uncoated samples could not be calculated accurately due to the significant transfer of the material from the counter body, the aluminium ball.

CHAPTER 5

5. CONCLUSION

For our project W-S-C coatings were deposited by DC magnetron sputtering technique. Three different coatings by varying carbon content were deposited on the H11 tool steel sample. The deposited coatings were subjected to scratch test, nano indentation test to identify find the hardness of the film, and coating characterization to understand the morphology and structure of the film. Reciprocating ball on disk test was performed at elevated temperature as well as at RT with aluminium ball as counter body. Following the tribological test wear track analysis of the coatings was done.

- Carbon content of the coating varied from 27.4 at. % to 35.4 at. % by applying different power supplied to the graphite target. WSC1010 with 27.4 at. % of C and lastly WSC1016 with 35.4 at.% of carbon were the three coatings used for this thesis. For the deposition two graphite target, one WS_2 and one Cr target was used for the deposition process. Thickness of the coating was between 1.28 µm to 1.53 µm.
- With increasing carbon content dense structure and featureless morphologies was observed. Columnar and porous structure was noticed for coating with less carbon content.
- Diffractograms of the coatings with richer C contents (>30%) or lower S contents (30% at. %) revealed an amorphous structure for X-ray diffraction, with a broad peak at 2θ = 33–50°.
- Increasing the carbon content resulted in increasing the hardness of the coatings, W-S-C coatings exhibit higher adhesion and have harder hardness values in the 5.6 – 5.8 GPa range than pure W–S with 50V biased voltage with only 2.8 GPa.
- With the increase of carbon content, critical loads of the coatings also increased. WSC1010 and WSC1016 had a comparable L_c1 and L_c2 of around 6N and 25N, respectively. However, for none of the sample L_c3 could be identified.
- W-S-C coating significantly reduced the galling of aluminium at RT as well as at elevated temperature. COF as low as 0.02 was observed for WSC1010 coating at 200°C.
- For WSC1010 and $WS_2$50V transfer of aluminium was not noticed even at 400°C. Most of the coated sample performed well at elevated temperature.

- WSC1010 coating could a viable solution for the prevention of aluminium at elevated temperature.
- It seems that lower C content performs better in terms of resisting galling and achieving lower COF.

CHAPTER 6

6. FUTURE RECOMMENDATION

The following future work is recommended for the systematic study of WSC coatings:

- Perform the test with a greater number of coatings with varying carbon content to find the optimum quantity of carbon that could suffice aluminium galling.

- Perform the test with aluminium pin to replicate the real-life scenario.

- Use of several types of commercially available aluminium alloys is highly recommended.

- Perform the tribological experiments with different normal loads.

- Conduct the Thermogravimetric analysis (TGA) of the coatings to understand the thermal stability and oxidation resistance.

- Analysis of ball wear and wear tracks extensively to understand the mechanism of galling and type of failure.

References

[1] "Tribological properties of PM212: A high-temperature, self-lubricating, powder metallurgy composite (Conference) | OSTI.GOV." https://www.osti.gov/biblio/7007298-tribological-properties-pm212-high-temperature-self-lubricating-powder-metallurgy-composite (accessed Jul. 02, 2022).

[2] S. Gupta, D. Filimonov, T. Palanisamy, T. El-Raghy, and M. W. Barsoum, "Ta2AlC and Cr2AlC Ag-based composites—New solid lubricant materials for use over a wide temperature range against Ni-based superalloys and alumina," *Wear*, vol. 262, no. 11–12, pp. 1479–1489, May 2007, doi: 10.1016/J.WEAR.2007.01.028.

[3] S. Aouadi, B. Luster, P. Kohli, … C. M.-S. and C., and undefined 2009, "Progress in the development of adaptive nitride-based coatings for high temperature tribological applications," *Elsevier*, Accessed: Jul. 02, 2022. [Online]. Available: https://www.sciencedirect.com/science/article/pii/S025789720900348X

[4] H. E. Sliney, "Solid lubricant materials for high temperatures—a review," *Tribology International*, vol. 15, no. 5, pp. 303–315, Oct. 1982, doi: 10.1016/0301-679X(82)90089-5.

[5] S. v. Prasad and J. S. Zabinski, "Tribology of tungsten disulphide (WS2): characterization of wear-induced transfer films," *J. Mater. Sci. Lett.*, vol. 11, no. 18, pp. 1413–1415, Jan. 1993, doi: 10.1007/bf00591592.

[6] A. Nossa, A. Cavaleiro, N. J. M. Carvalho, B. J. Kooi, and J. T. M. de Hosson, "On the microstructure of tungsten disulfide films alloyed with carbon and nitrogen," *Thin Solid Films*, vol. 484, no. 1–2, pp. 389–395, Jul. 2005, doi: 10.1016/j.tsf.2005.02.018.

[7] A. R. Lansdown, "Molybdenum disulphide lubrication," p. 380, 1999.

[8] C. Donnet and A. Erdemir, "Diamond-like carbon films: A historical overview," *Tribology of Diamond-Like Carbon Films: Fundamentals and Applications*, pp. 1–10, 2008, doi: 10.1007/978-0-387-49891-1/COVER.

[9] S. v. Prasad, N. T. McDevitt, and J. S. Zabinski, "Tribology of tungsten disulfide films in humid environments:: The role of a tailored metal-matrix composite substrate," *Wear*, vol. 230, no. 1, pp. 24–34, May 1999, doi: 10.1016/S0043-1648(99)00082-4.

[10] J. Moser, F. Lévy, and F. Bussy, "Composition and growth mode of MoSx sputtered films," *Journal of Vacuum Science & Technology A: Vacuum, Surfaces, and Films*, vol. 12, no. 2, p. 494, Jun. 1998, doi: 10.1116/1.579157.

[11] T. Polcar, M. Evaristo, M. Stueber, and A. Cavaleiro, "Synthesis and structural properties of Mo-Se-C sputtered coatings," *Surface and Coatings Technology*, vol. 202, no. 11, pp. 2418–2422, Feb. 2008, doi: 10.1016/J.SURFCOAT.2007.08.019.

[12] A. Madhukar, "Structural classification of layered dichalcogenides of group IV B, V B and VI B transition metals," *Solid State Communications*, vol. 16, no. 4, pp. 383–388, Feb. 1975, doi: 10.1016/0038-1098(75)90092-7.

[13] T. Polcar and A. Cavaleiro, “Review on self-lubricant transition metal dichalcogenide nanocomposite coatings alloyed with carbon,” *Surface and Coatings Technology*, vol. 206, no. 4, pp. 686–695, Nov. 2011, doi: 10.1016/J.SURFCOAT.2011.03.004.
[14] W. Choi, N. Choudhary, G. H. Han, J. Park, D. Akinwande, and Y. H. Lee, “Recent development of two-dimensional transition metal dichalcogenides and their applications,” *Materials Today*, vol. 20, no. 3, pp. 116–130, Apr. 2017, doi: 10.1016/J.MATTOD.2016.10.002.
[15] A. A. Voevodin, J. P. O’Neill, and J. S. Zabinski, “Nanocomposite tribological coatings for aerospace applications,” *Surface and Coatings Technology*, vol. 116–119, pp. 36–45, Sep. 1999, doi: 10.1016/S0257-8972(99)00228-5.
[16] T. Polcar and A. Cavaleiro, “Self-adaptive low friction coatings based on transition metal dichalcogenides,” *Thin Solid Films*, vol. 519, no. 12, pp. 4037–4044, Apr. 2011, doi: 10.1016/J.TSF.2011.01.180.
[17] D. Lundin, T. Minea, and J. T. Gudmundsson, “High power impulse magnetron sputtering : fundamentals, technologies, challenges and applications”.
[18] J. Caessa, T. Vuchkov, T. bin Yaqub, and A. Cavaleiro, “On the Microstructural, Mechanical and Tribological Properties of Mo-Se-C Coatings and Their Potential for Friction Reduction against Rubber,” *Materials 2021, Vol. 14, Page 1336*, vol. 14, no. 6, p. 1336, Mar. 2021, doi: 10.3390/MA14061336.
[19] M. Evaristo, A. Nossa, and A. Cavaleiro, “W-S-C sputtered films: Influence of the carbon alloying method on the mechanical properties,” *Surface and Coatings Technology*, vol. 200, no. 1-4 SPEC. ISS., pp. 1076–1079, Oct. 2005, doi: 10.1016/j.surfcoat.2005.02.039.
[20] A. Nossa and A. Cavaleiro, “Mechanical behaviour of W–S–N and W–S–C sputtered coatings deposited with a Ti interlayer,” *Surface and Coatings Technology*, vol. 163–164, pp. 552–560, Jan. 2003, doi: 10.1016/S0257-8972(02)00622-9.
[21] T. bin Yaqub, S. Bruyere, J. F. Pierson, T. Vuchkov, and A. Cavaleiro, “Insights into the wear track evolution with sliding cycles of carbon-alloyed transition metal dichalcogenide coatings,” *Surface and Coatings Technology*, vol. 403, p. 126360, Dec. 2020, doi: 10.1016/J.SURFCOAT.2020.126360.
[22] H. Xiao and S. Liu, “2D nanomaterials as lubricant additive: A review,” *Materials & Design*, vol. 135, pp. 319–332, Dec. 2017, doi: 10.1016/J.MATDES.2017.09.029.
[23] F. P. Bowden and D. Tabor, “MECHANISM OF METALLIC FRICTION,” *Nature 1942 150:3798*, vol. 150, no. 3798, pp. 197–199, 1942, doi: 10.1038/150197a0.
[24] Q. Li, Q. Zhou, L. Shi, Q. Chen, and J. Wang, “Recent advances in oxidation and degradation mechanisms of ultrathin 2D materials under ambient conditions and their passivation strategies,” *Journal of Materials Chemistry A*, vol. 7, no. 9, pp. 4291–4312, Feb. 2019, doi: 10.1039/C8TA10306B.
[25] H. S. Khare and D. L. Burris, “The effects of environmental water and oxygen on the temperature-dependent friction of sputtered molybdenum disulfide,” *Tribology Letters*, vol. 52, no. 3, pp. 485–493, Dec. 2013, doi: 10.1007/S11249-013-0233-8.
[26] T. W. Scharf and S. v. Prasad, “Solid lubricants: A review,” *Journal of Materials Science*, vol. 48, no. 2, pp. 511–531, Jan. 2013, doi: 10.1007/S10853-012-7038-2.
[27] F. Gustavsson and S. Jacobson, “Diverse mechanisms of friction induced self-organisation into a low-friction material – An overview of WS2 tribofilm formation,” *Tribology International*, vol. 101, pp. 340–347, Sep. 2016, doi: 10.1016/J.TRIBOINT.2016.04.029.

[28] T. W. Scharf, A. Rajendran, R. Banerjee, and F. Sequeda, “Growth, structure and friction behavior of titanium doped tungsten disulphide (Ti-WS2) nanocomposite thin films,” *Thin Solid Films*, vol. 517, no. 19, pp. 5666–5675, Aug. 2009, doi: 10.1016/J.TSF.2009.02.103.
[29] J. P. Hirvonen, J. Koskinen, J. R. Jervis, and M. Nastasi, “Present progress in the development of low friction coatings,” *Surface and Coatings Technology*, vol. 80, no. 1–2, pp. 139–150, 1996, doi: 10.1016/0257-8972(95)02701-7.
[30] W. Lauwerens *et al.*, “Humidity resistant MoSx films prepared by pulsed magnetron sputtering,” *Surface and Coatings Technology*, vol. 131, no. 1–3, pp. 216–221, Sep. 2000, doi: 10.1016/S0257-8972(00)00796-9.
[31] G. Salitra, G. Hodes, E. Klein, and R. Tenne, “Highly oriented WSe2 thin films prepared by selenization of evaporated WO3,” *Thin Solid Films*, vol. 245, no. 1–2, pp. 180–185, Jun. 1994, doi: 10.1016/0040-6090(94)90896-6.
[32] S. Prasad and J. Zabinski, “Super slippery solids,” *Nature 1997 387:6635*, vol. 387, no. 6635, pp. 761–763, 1997, doi: 10.1038/42820.
[33] T. Polcar and A. Cavaleiro, “Review on self-lubricant transition metal dichalcogenide nanocomposite coatings alloyed with carbon,” *Surface and Coatings Technology*, vol. 206, no. 4, pp. 686–695, Nov. 2011, doi: 10.1016/J.SURFCOAT.2011.03.004.
[34] V. Buck, “Preparation and properties of different types of sputtered MoS2 films,” *Wear*, vol. 114, no. 3, pp. 263–274, Feb. 1987, doi: 10.1016/0043-1648(87)90116-5.
[35] J. Moser and F. Lèvy, “MoS2-x lubricating films: structure and wear mechanisms investigated by cross-sectional transmission electron microscopy,” *Thin Solid Films*, vol. 228, no. 1–2, pp. 257–260, May 1993, doi: 10.1016/0040-6090(93)90611-R.
[36] T. Polcar and A. Cavaleiro, “Review on self-lubricant transition metal dichalcogenide nanocomposite coatings alloyed with carbon,” *Surface and Coatings Technology*, vol. 206, no. 4, pp. 686–695, Nov. 2011, doi: 10.1016/J.SURFCOAT.2011.03.004.
[37] T. Vuchkov, T. bin Yaqub, M. Evaristo, and A. Cavaleiro, “Synthesis, Microstructural, and Mechano-Tribological Properties of Self-Lubricating W-S-C(H) Thin Films Deposited by Different RF Magnetron Sputtering Procedures,” *Coatings 2020, Vol. 10, Page 272*, vol. 10, no. 3, p. 272, Mar. 2020, doi: 10.3390/COATINGS10030272.
[38] E. Rabinowicz, “Friction and Wear of Materials (2nd Edition),” p. 336, 1995, Accessed: Jul. 03, 2022. [Online]. Available: http://atc.sjf.stuba.sk/files/mechanika_vms_ADAMS/Contact_Table.pdf
[39] J. Pujante, M. Vilaseca, D. Casellas, and M. D. Riera, “The role of adhesive forces and mechanical interaction on material transfer in hot forming of aluminium,” *Tribology Letters*, vol. 59, no. 1, Jul. 2015, doi: 10.1007/S11249-015-0542-1.
[40] J. Heinrichs and S. Jacobson, “Laboratory test simulation of galling in cold forming of aluminium,” *Wear*, vol. 267, no. 12, pp. 2278–2286, Dec. 2009, doi: 10.1016/J.WEAR.2009.04.006.
[41] J. Heinrichs, M. Olsson, and S. Jacobson, “New understanding of the initiation of material transfer and transfer layer build-up in metal forming—In situ studies in the SEM,” *Wear*, vol. 292–293, pp. 61–73, Jul. 2012, doi: 10.1016/J.WEAR.2012.05.032.
[42] O. Gali, “Micro-mechanisms of Surface Defects Induced on Aluminum Alloys during Plastic Deformation at Elevated Temperatures,” *Electronic Theses and Dissertations*, Apr. 2017, Accessed: Jul. 03, 2022. [Online]. Available: https://scholar.uwindsor.ca/etd/5936

[43] X. Fan, Z. He, S. Yuan, and K. Zheng, “Experimental investigation on hot forming-quenching integrated process of 6A02 aluminum alloy sheet,” *Materials Science and Engineering A*, vol. 573, pp. 154–160, Jun. 2013, doi: 10.1016/J.MSEA.2013.02.058.
[44] K. Zheng, J. Lee, W. Xiao, B. Wang, and J. Lin, “Experimental investigations of the in-die quenching efficiency and die surface temperature of hot stamping aluminium alloys,” *Metals (Basel)*, vol. 8, no. 4, Apr. 2018, doi: 10.3390/MET8040231.
[45] D. K. Dwivedi, “Sliding temperature and wear behaviour of cast Al-Si-Mg alloys,” *Materials Science and Engineering A*, vol. 382, no. 1–2, pp. 328–334, Sep. 2004, doi: 10.1016/J.MSEA.2004.05.014.
[46] J. Pujante, L. Pelcastre, M. Vilaseca, D. Casellas, and B. Prakash, “Investigations into wear and galling mechanism of aluminium alloy-tool steel tribopair at different temperatures,” *Wear*, vol. 308, no. 1–2, pp. 193–198, Nov. 2013, doi: 10.1016/J.WEAR.2013.06.015.
[47] J. Mendiguren, E. S. de Argandona, and L. Galdos, “Hot stamping of AA7075 aluminum sheets,” *IOP Conference Series: Materials Science and Engineering*, vol. 159, no. 1, p. 012026, Nov. 2016, doi: 10.1088/1757-899X/159/1/012026.
[48] J. H. Beynon, “Tribology of hot metal forming,” *Tribology International*, vol. 31, no. 1–3, pp. 73–77, Jan. 1998, doi: 10.1016/S0301-679X(98)00009-7.
[49] “The wear of metals under unlubricated conditions,” *Proceedings of the Royal Society of London. Series A. Mathematical and Physical Sciences*, vol. 236, no. 1206, pp. 397–410, Aug. 1956, doi: 10.1098/RSPA.1956.0144.
[50] S. Das and S. K. Biswas, “Boundary lubricated tribology of an aluminium-silicon alloy sliding against steel,” *Tribology Letters*, vol. 17, no. 3, pp. 623–628, Oct. 2004, doi: 10.1023/B:TRIL.0000044512.48967.02.
[51] S. Das, A. T. Morales, A. R. Riahi, X. Meng-Burany, and A. T. Alpas, “Role of plastic deformation on elevated temperature tribological behavior of an Al-Mg alloy (AA5083): A friction mapping approach,” *Metallurgical and Materials Transactions A: Physical Metallurgy and Materials Science*, vol. 42, no. 8, pp. 2384–2401, Aug. 2011, doi: 10.1007/S11661-011-0649-4.
[52] J. Zhang and A. T. Alpas, “Transition between mild and severe wear in aluminium alloys,” *Acta Materialia*, vol. 45, no. 2, pp. 513–528, Feb. 1997, doi: 10.1016/S1359-6454(96)00191-7.
[53] C. Subramanian, “Wear properties of aluminium-based alloys,” *Surface Engineering of Light Alloys: Aluminium, Magnesium and Titanium Alloys*, pp. 40–57, Jan. 2010, doi: 10.1533/9781845699451.1.40.
[54] T. Vuchkov, M. Evaristo, T. bin Yaqub, and A. Cavaleiro, “The effect of substrate location on the composition, microstructure and mechano-tribological properties of W-S-C coatings deposited by magnetron sputtering,” *Surface and Coatings Technology*, vol. 386, p. 125481, Mar. 2020, doi: 10.1016/J.SURFCOAT.2020.125481.
[55] A. A. Voevodin, T. A. Fitz, J. J. Hu, and J. S. Zabinski, “Nanocomposite tribological coatings with ‘chameleon’ surface adaptation,” *Journal of Vacuum Science & Technology A: Vacuum, Surfaces, and Films*, vol. 20, no. 4, p. 1434, Jun. 2002, doi: 10.1116/1.1487875.
[56] T. Vuchkov, M. Evaristo, T. bin Yaqub, T. Polcar, and A. Cavaleiro, “Synthesis, microstructure and mechanical properties of W–S–C self-lubricant thin films deposited by

magnetron sputtering," *Tribology International*, vol. 150, Oct. 2020, doi: 10.1016/J.TRIBOINT.2020.106363.
[57] L. E. Rumaner, T. Tazawa, and F. S. Ohuchi, "Compositional change of (0001) WS2 surfaces induced by ion beam bombardment with energies between 100 and 1500 eV," *Journal of Vacuum Science & Technology A: Vacuum, Surfaces, and Films*, vol. 12, no. 4, p. 2451, Jun. 1998, doi: 10.1116/1.579192.
[58] E. Särhammar *et al.*, "Mechanisms for compositional variations of coatings sputtered from a WS2 target," *Surface and Coatings Technology*, vol. 252, pp. 186–190, Aug. 2014, doi: 10.1016/J.SURFCOAT.2014.04.066.
[59] A. Nossa and A. Cavaleiro, "Chemical and physical characterization of C(N)-doped W–S sputtered films," *Journal of Materials Research 2004 19:8*, vol. 19, no. 8, pp. 2356–2365, Aug. 2004, doi: 10.1557/JMR.2004.0293.
[60] J. C. Oliveira, F. Fernandes, F. Ferreira, and A. Cavaleiro, "Tailoring the nanostructure of Ti–Si–N thin films by HiPIMS in deep oscillation magnetron sputtering (DOMS) mode," *Surface and Coatings Technology*, vol. 264, pp. 140–149, Feb. 2015, doi: 10.1016/J.SURFCOAT.2014.12.065.
[61] J. Moser and F. Lévy, "Random stacking in MoS2−x sputtered thin films," *Thin Solid Films*, vol. 240, no. 1–2, pp. 56–59, Mar. 1994, doi: 10.1016/0040-6090(94)90693-9.
[62] A. W. Wright, "On a new process for the electrical deposition of metals, and for constructing metal-covered glass specula," *American Journal of Science*, vol. s3-14, no. 81, pp. 169–178, Sep. 1877, doi: 10.2475/AJS.S3-14.81.169.
[63] J. Sundberg, "Triboactive Low-Friction Coatings Based on Sulfides and Carbides," 2014.
[64] M. Evaristo, A. Nossa, and A. Cavaleiro, "W–S–C sputtered films: Influence of the carbon alloying method on the mechanical properties," *Surface and Coatings Technology*, vol. 200, no. 1–4, pp. 1076–1079, Oct. 2005, doi: 10.1016/J.SURFCOAT.2005.02.039.
[65] G. Zhang, Y. Xu, D. Xu, D. Wang, Y. Xue, and W. Su, "Pressure-induced crystallization of amorphous SiO2 with silicon–hydroxy group and the quick synthesis of coesite under lower temperature," *https://doi.org/10.1080/08957950802510091*, vol. 28, no. 4, pp. 641–650, Dec. 2008, doi: 10.1080/08957950802510091.
[66] C. Donnette and A. Erdemir, "Diamond-like carbon films: A historical overview," *Tribology of Diamond-Like Carbon Films: Fundamentals and Applications*, pp. 1–10, 2008, doi: 10.1007/978-0-387-49891-1/COVER.
[67] I. Petrov, P. B. Barna, L. Hultman, and J. E. Greene, "Microstructural evolution during film growth," *Journal of Vacuum Science & Technology A: Vacuum, Surfaces, and Films*, vol. 21, no. 5, pp. S117–S128, Sep. 2003, doi: 10.1116/1.1601610.
[68] J. Stallard, S. Poulat, and D. G. Teer, "The study of the adhesion of a TiN coating on steel and titanium alloy substrates using a multi-mode scratch tester," *Tribology International*, vol. 39, no. 2, pp. 159–166, Feb. 2006, doi: 10.1016/J.TRIBOINT.2005.04.011.
[69] P. Mutafov, M. Evaristo, A. Cavaleiro, and T. Polcar, "Structure, mechanical and tribological properties of self-lubricant W-S-N coatings," *Surface and Coatings Technology*, vol. 261, pp. 7–14, Jan. 2015, doi: 10.1016/J.SURFCOAT.2014.11.074.
[70] "(PDF) Improvement of the tribological performance of WSCF coatings under dry and lubricated conditions Submitted in Partial Fulfilment of the Requirements for the Joint European Master in Tribology of Surfaces and Interfaces." https://www.researchgate.net/publication/355295775_Improvement_of_the_tribological_performance_of_WSCF_coatings_under_dry_and_lubricated_conditions_Submitted_in_Pa

rtial_Fulfilment_of_the_Requirements_for_the_Joint_European_Master_in_Tribology_of_Surfa (accessed Jul. 04, 2022).
[71] "Adhesion tests [SubsTech]." http://www.substech.com/dokuwiki/doku.php?id=adhesion_tests (accessed Jul. 11, 2022).